JOURNAL OF PETROLOGY | VOLUME 49 | NUMBER 2 | PAGES 295–313 | 2008 | doi:10.1093/petrology/egm082

Origin of Fe–Ti Oxide Ores in Mafic Intrusions: Evidence from the Panzhihua Intrusion, SW China

KWAN-NANG PANG[1]*, MEI-FU ZHOU[1], DONALD LINDSLEY[2], DONGGAO ZHAO[3] AND JOHN MALPAS[1]

[1]DEPARTMENT OF EARTH SCIENCES, THE UNIVERSITY OF HONG KONG, HONG KONG, CHINA
[2]DEPARTMENT OF GEOSCIENCES, STONY BROOK UNIVERSITY, STONY BROOK, NY 11794-2100, USA
[3]ELECTRON MICROSCOPY CENTER AND DEPARTMENT OF GEOLOGICAL SCIENCES, THE UNIVERSITY OF SOUTH CAROLINA, COLUMBIA, SC 29208, USA

RECEIVED NOVEMBER 8, 2006; ACCEPTED DECEMBER 3, 2007
ADVANCE ACCESS PUBLICATION DECEMBER 26, 2007

Economic concentrations of Fe–Ti oxides occur as massive, conformable lenses or layers in the lower part of the Panzhihua intrusion, Emeishan Large Igneous Province, SW China. Mineral chemistry, textures and QUILF equilibria indicate that oxides in rocks of the intrusion were subjected to extensive subsolidus re-equilibration and exsolution. The primary oxide, reconstructed from compositions of titanomagnetite in the ores and associated intergrowths, is an aluminous titanomagnetite (Usp_{40}*) with 40 wt % FeO, 34 wt % Fe_2O_3, 16·5 wt % TiO_2, 5·3 wt % Al_2O_3, 3·5 wt % MgO and 0·5 wt % MnO. This composition is similar to the bulk composition of the oxide ore, as inferred from whole-rock data. This similarity strongly suggests that the ores formed from accumulation of titanomagnetite crystals, not from immiscible oxide melt as proposed in earlier studies. The occurrence of oxide ores in the lower parts of the Panzhihua intrusion is best explained by settling and sorting of dense titanomagnetite in the ferrogabbroic parental magma. This magma must have crystallized Fe–Ti oxides relatively early and abundantly, and is likely to have been enriched in Fe and Ti but poor in SiO_2. These features are consistent with fractionation of mantle-derived melts under relatively high pressures (~10 kbar), followed by emplacement of the residual magma at ~5 kbar. This study provides definitive field and geochemical evidence that Fe–Ti oxide ores can form by accumulation in ferrogabbro. We suggest that many other massive Fe–Ti oxide deposits may have formed in a similar fashion and that high concentrations of phosphorus or carbon, or periodic fluctuation of* fO_2 *in the magma, are of secondary importance in ore formation.*

KEY WORDS: *ELIP; Fe–Ti oxide ore; layered intrusion; Panzhihua; QUILF*

INTRODUCTION

Magmatic Fe–Ti oxide ores are commonly associated with or hosted in mafic intrusions or Proterozoic anorthosite complexes (Bateman, 1951; Lister, 1966; Force, 1991). These ores are important sources of Fe, Ti, V and P, and are generally characterized by complex field and textural relations. Field evidence shows that they occur either as disseminated oxides in homogeneous silicate rocks, or as veins, lenses or layers of massive Fe–Ti oxides ± apatite (i.e. nelsonite) that are in sharp contact with their host rocks (e.g. Willemse, 1969; Duchesne, 1999). In addition, oxide minerals in these rocks commonly display curved boundaries against coexisting silicate minerals (von Gruenewaldt, 1993; Duchesne, 1999). The origin of these ores has been controversial partly as a result of such diversity. Two attractive but contrasting models proposed for their formation include sorting of Fe–Ti oxide crystals from magmas (Emslie, 1975; Ashwal, 1978; Duchesne, 1999; Charlier *et al.*, 2006), and accumulation of oxide melts that resulted from immiscible separation in magmas (Lister, 1966; Kolker, 1982; Force, 1991; von Gruenewaldt, 1993).

A unique feature of Fe–Ti oxide ores and associated intrusive rocks is their magmatic origin. They underwent slow

*Corresponding author. Telephone: (852)-28578521. Fax: (852)-25176912. E-mail: knpang@graduate.hku.hk

cooling in crustal magma chambers, a process that modifies both the original composition and textures of the oxide minerals present in them (Frost & Lindsley, 1991, 1992). This leads to a loss of magmatic information that is critical in the understanding of the origin of these ores. The present study focuses on the textures, mineralogy and chemistry of oxide minerals in rocks of the Panzhihua intrusion, Emeishan Large Igneous Province (ELIP), SW China. The intrusion hosts a significant Fe–Ti oxide deposit and provides a good opportunity to investigate how such ores formed. Here, we provide compositional data for oxide minerals in the rocks of the Panzhihua intrusion. Using these data, we investigate the cooling history of these rocks and the origin of Fe–Ti oxide ores.

GEOLOGICAL BACKGROUND

Regional geology

Southwest China includes the Yangtze Block to the east and the Tibetan Plateau to the west (Fig. 1, inset). The region where the ELIP is exposed lies close to the western margin of the Yangtze Block and the eastern margin of the Tibetan Plateau. The ELIP consists of huge volumes of flood basalts, known as the Emeishan basalts, and a diverse assemblage of plutonic rocks that resulted from mantle plume-related magmatism in the Late Permian at ~260 Ma (Chung & Jahn, 1995; Xu *et al.*, 2001; Zhou *et al.*, 2002; Xiao *et al.*, 2004; Zhang *et al.*, 2006). The Emeishan basalts are mainly exposed in the Sichuan, Guizhou and Yunnan Provinces, covering an area of $\sim 0{\cdot}5 \times 10^6\,km^2$. In the Panzhihua–Xichang (Pan–Xi) region of the western ELIP, a series of north–south-trending faults have exposed the plutonic rocks, including felsic and mafic–ultramafic intrusions, over a considerable range of emplacement depths.

Mafic–ultramafic intrusions in the Pan–Xi region include the Panzhihua, Hongge, Baima, Taihe, and Xinjie intrusions. Zhou *et al.* (2002, 2005) and Zhong & Zhu (2006) showed that the intrusions are coeval with the associated Emeishan basalts, based on sensitive high-resolution ion microprobe U–Pb zircon geochronology of the intrusions and of the dykes that fed the basalts. The mafic–ultramafic intrusions are characterized by well-developed igneous layering. They commonly contain stratiform Fe–Ti oxide orebodies in the lower parts of the intrusions, or as cyclic units within the intrusions. The Xinjie and Hongge intrusions contain ultramafic portions, whereas the Panzhihua, Baima, and Taihe intrusions are mafic throughout. These intrusions represent an important Fe–Ti–V resource in China. The total estimated reserve exceeds 6000 Mt of ore with 27–45% FeO, 11–12 wt % TiO_2, and 0·24–0·3 wt % V_2O_5 (Ma *et al.*, 2003). The Panzhihua intrusion has been mined for Fe–Ti oxides for more than 30 years and mining activity is still continuing at present. Other intrusions are currently under re-evaluation.

Geology of the Panzhihua intrusion

The Panzhihua layered gabbroic intrusion is a 19 km long sill that strikes NE–SW and is cut by a series of NW–SE-trending faults into the Zujiabaobao, Lanjiahuoshan, Jianshan, Daomakan, Gongshan and Nalaqing segments (Fig. 2). The igneous layering strikes parallel to the long axis of the intrusion and in general dips 50–60° NW. The exposed gabbroic cumulates have a maximum thickness of ~2 km. The footwall of the intrusion consists of Neoproterozoic dolomitic limestone (Dengying Formation), locally transformed to marble as a result of contact metamorphism. Abundant marble xenoliths close to the basal contact suggest that the Panzhihua magma was directly emplaced into the carbonate country rocks. The roof contact is not exposed, but is mapped as a thrust fault against the hanging-wall syenite (Fig. 2). Field relations indicate that the syenite intruded the nearby Emeishan basalts. The Panzhihua intrusion and associated syenite are unconformably overlain by Triassic terrigenous sedimentary rocks.

The zonal division and the variations in mineral composition of the Panzhihua intrusion are summarized in Fig. 3. These data will be discussed in detail in a subsequent publication. The Panzhihua intrusion is divided into four zones from the base upwards: the Marginal zone (MGZ), Lower zone (LZ), Middle zone (MZ) and Upper zone (UZ) (Ma *et al.*, 2001). These divisions were adopted by mining geologists regarding the gross structure and/or texture observed in the rocks of the intrusion, but do not reflect the appearance or disappearance of cumulus minerals. We follow this subdivision for consistency with a previous study by Zhou *et al.* (2005). The MGZ consists mainly of microgabbro interpreted to be the chilled base of the intrusion. The LZ is composed of gabbros and oxide-gabbros that are coarse-grained and without a prominent layered structure. The LZ locally contains pegmatoidal facies that are generally absent in the overlying zones. The MZ is also composed of gabbro and oxide-gabbro, but with medium grain size, well-developed igneous layering and magmatic foliation compared with the LZ rocks. The layered structure is represented by alternative melanocratic layers rich in mafic minerals and leucocratic layers rich in plagioclase. The thicknesses of these layers range from a few centimeters to several meters. The magmatic foliation is marked by the preferred orientation of plagioclase subparallel to that of the layering. In this study, the MZ is subdivided into MZa and MZb based on the appearance of cumulus apatite (Fig. 3). The UZ is composed mainly of leucogabbro with minor layers of olivine gabbro, olivine clinopyroxenite and anorthosite.

In this study, a three-fold lithological classification has been adopted for rocks of the Panzhihua intrusion and this is used throughout: gabbro (0–25 vol. % Fe–Ti oxides), oxide-gabbro (25–50 vol. % Fe–Ti oxides), and Fe–Ti oxide ores (50–100 vol. % Fe–Ti oxides). There is a spectrum of modal mineralogy from Cpx + Plag ~100 vol. % (gabbro)

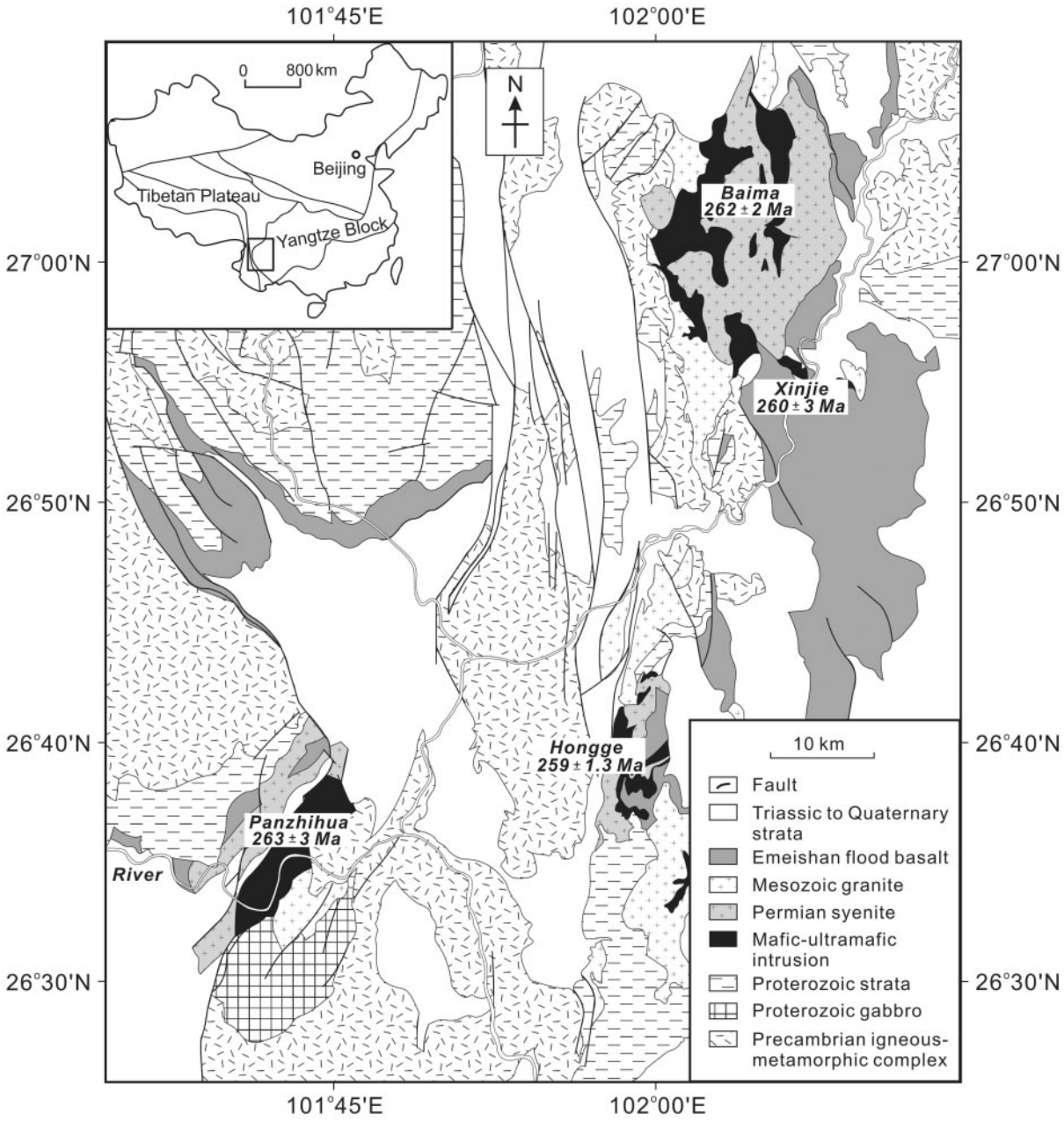

Fig. 1. Generalized geological map of the Pan–Xi area, Emeishan Large Igneous Province, SW China showing the distribution of mafic–ultramafic intrusions that host Fe–Ti oxide mineralization (e.g. Panzhihua, Hongge, Baima). Inset shows the location of the study area within China.

to Mt (+ minor Ilm) ~100 vol. % (ores). All the rocks contain minor olivine ranging from ~5 to 20 vol. % in abundance, but this does not affect the above classification.

Contact relations of the oxide bodies

Massive or semi-massive Fe–Ti oxide bodies have different sizes and morphologies in the MGZ, LZ and locally in the lower part of the MZa of the Panzhihua intrusion. For example, some of them occur as centimeter-scale ore bands that appear intact in homogeneous silicate rocks (Fig. 4a). The silicate rocks commonly contain substantial amounts of Fe–Ti oxides, resulting in a gradational appearance in contact with the ore bands. Other oxide orebodies occur as conformable masses that are in sharp contact with adjacent silicate rocks, including thick (~20–60 m) lenticular masses (Fig. 4b), dyke-like bodies (Fig. 4c) and thin tabular sheets (Fig. 4d). Most contacts between the conformable orebodies and the adjacent silicate rocks are planar, with orientation similar to the igneous layering (Fig. 4b and d).

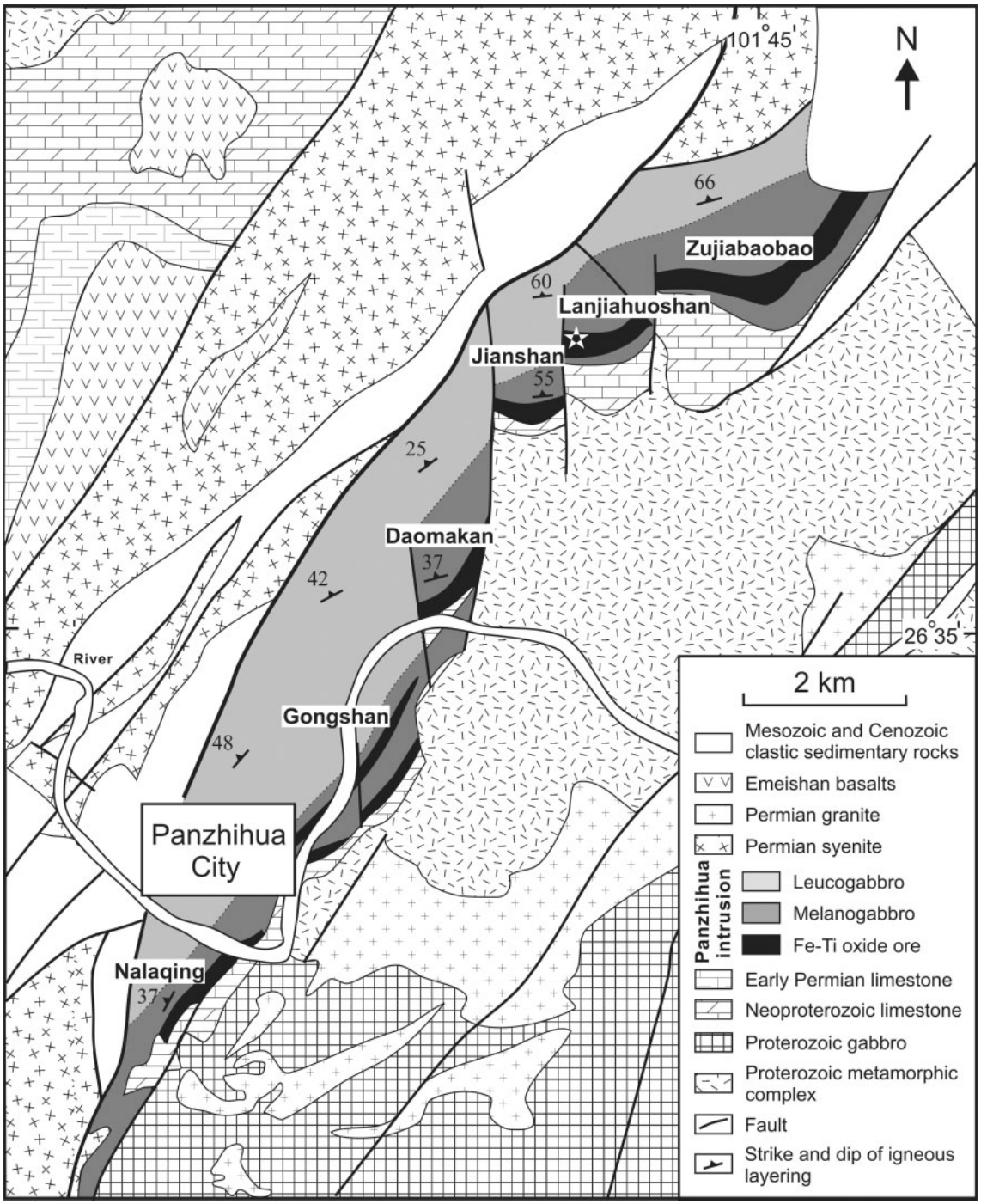

Fig. 2. Geological map of the Panzhihua intrusion (modified after Zhou *et al.*, 2005). The star indicates the location of the Lanjiahuoshan opencast mine.

PETROGRAPHY

The microgabbro in the MGZ of the Panzhihua intrusion contains clinopyroxene and plagioclase ± hornblende, with minor olivine, titanomagnetite, ilmenite and apatite. It is characterized by an equigranular texture with grain sizes between 0·2 to 0·5 mm. Some porphyritic microgabbros contain larger grains of clinopyroxene and plagioclase set in a matrix of the above minerals. Gabbro and oxide-gabbro from the LZ, MZ and UZ of the intrusion contain a mineral assemblage of olivine, clinopyroxene, plagioclase, titanomagnetite and ilmenite, with minor hornblende, apatite, pyrrhotite and pentlandite. Primary cumulus textures of

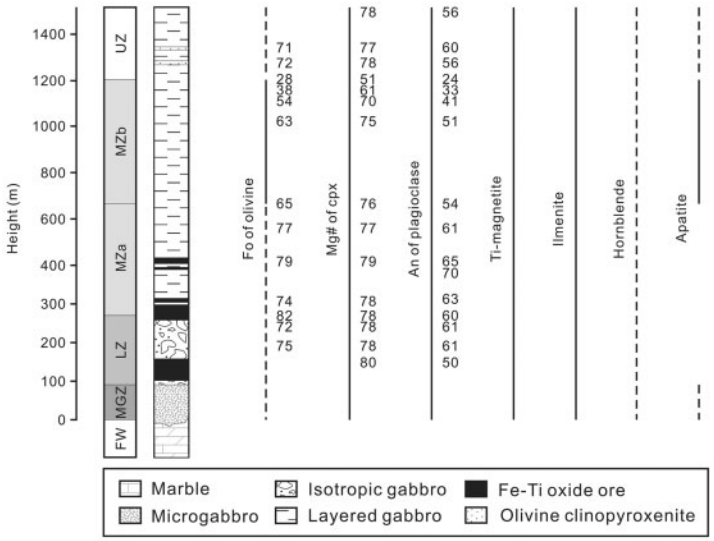

Fig. 3. Generalized stratigraphic section, showing the mineral occurrence and composition in the Panzhihua intrusion (K.-N. Pang & M.-F. Zhou, unpublished data). FW, footwall; MGZ, Marginal zone; LZ, Lower zone; MZa, Middle zone a; MZb, Middle zone b; UZ, Upper zone. Continuous line indicates ubiquitous occurrence; dashed line indicates sporadic occurrence.

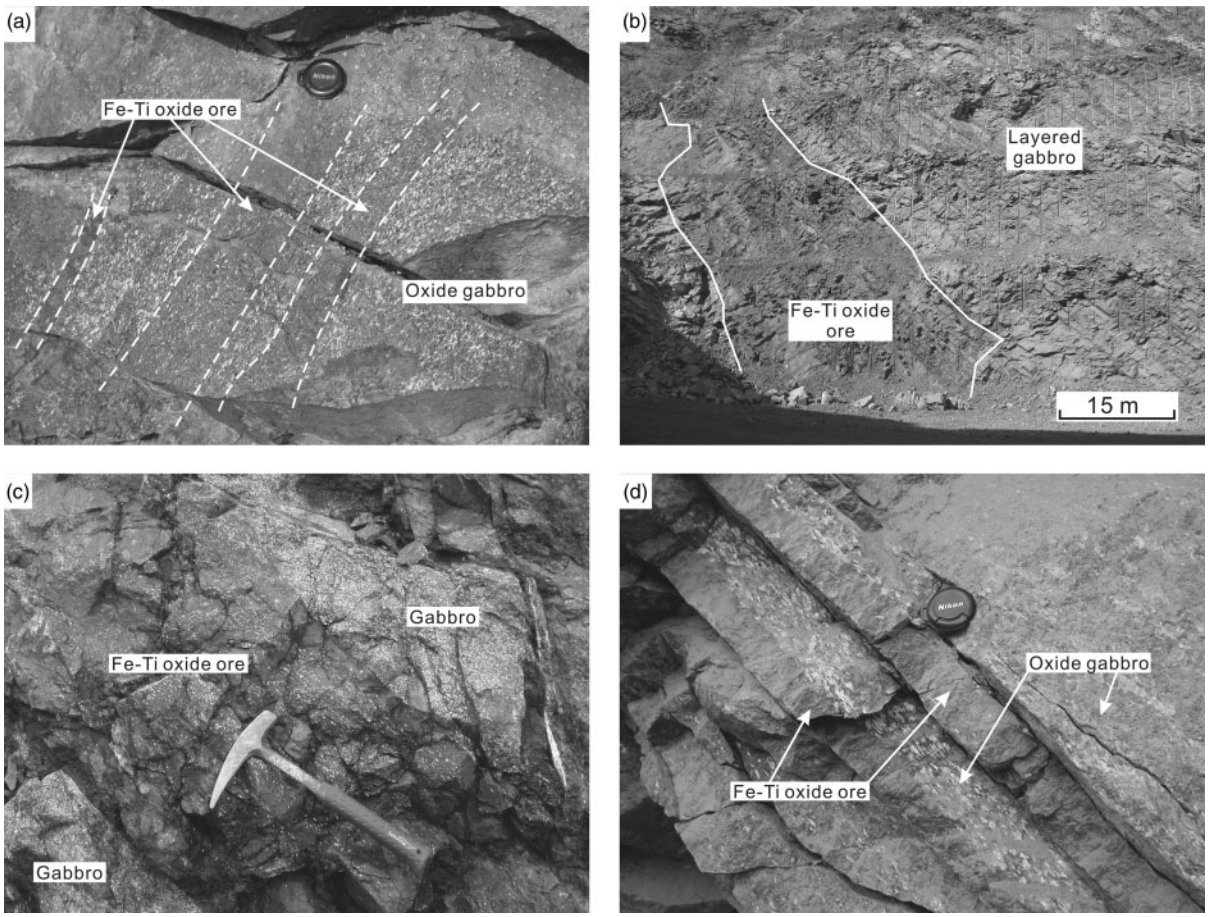

Fig. 4. Field relations between oxide bodies and their host rocks. (a) Centimeter-scale bands of oxide ore that appear intact within silicate host-rocks at the Nalaqing mine. (b) A thick, lenticular body of Fe–Ti oxides in sharp contact with layered gabbro in MZa at the Jianshan mine. (c) A dyke-like body of Fe–Ti oxides cutting gabbro at the Jianshan mine. (d) Thin tabular sheets of Fe–Ti oxides in sharp contact with oxide gabbro in MZa at the Jianshan mine.

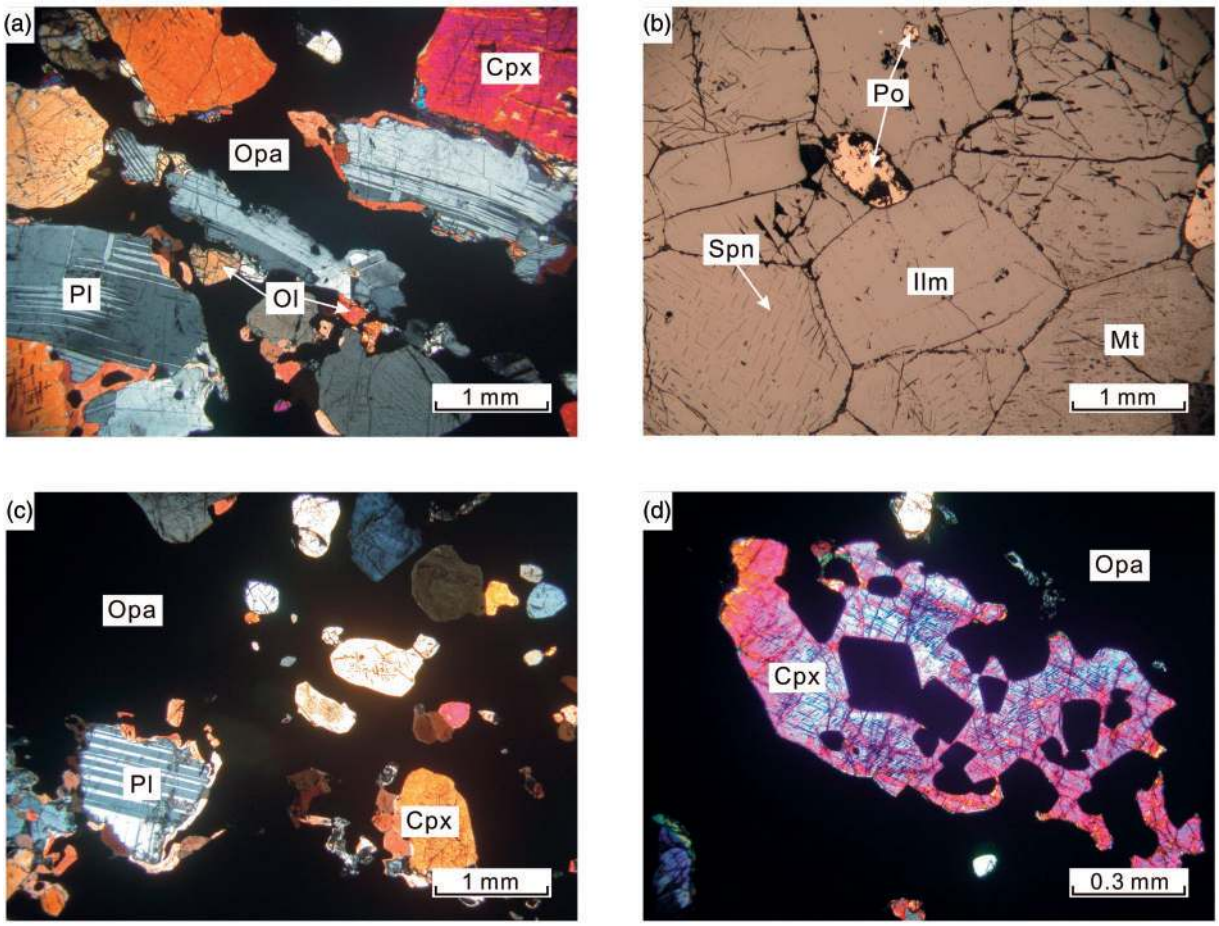

Fig. 5. Thin-section textures of Fe–Ti oxides in the rocks of the Panzhihua intrusion. (a) Oxide-gabbro consisting of cumulus clinopyroxene and plagioclase surrounded by interstitial Fe–Ti oxides. (b) Grains of polygonal magnetite and ilmenite with boundaries that meet at ~120° triple junctions in Fe–Ti oxide ore; the presence of hercynitic spinel lamellae in the magnetite host should be noted. (c) Oxide ore containing isolated grains of clinopyroxene and plagioclase in an oxide matrix. (d) Euhedral magnetite inclusions in a clinopyroxene grain in Fe–Ti oxide ore. Cpx, clinopyroxene; Ilm, ilmenite; Mt, magnetite; Ol, olivine; Opa, opaque oxides; Pl, plagioclase; Po, pyrrhotite; Spn, hercynitic spinel.

olivine, clinopyroxene and plagioclase are rarely preserved; the major evidence for the cumulate nature of the rocks is the presence of layering. Subsolidus recrystallization is evident, especially for plagioclase, which occurs as aggregates of small grains with well-annealed junctions. As a result, the gabbros are characterized by a large range in grain size. Iron–titanium oxides occur as interstitial fillings between the silicate minerals in the gabbros (Fig. 5a), or as an interconnected matrix of aggregated oxide grains surrounding the silicate minerals in the oxide-gabbros. The oxide assemblage in rocks of the MGZ, LZ and MZa is dominated by titanomagnetite, whereas that in rocks of the MZb and UZ consists of both titanomagnetite and ilmenite in subequal amounts. Coarse-grained plagioclase exhibits high-temperature deformation in the form of curved polysynthetic twinning. Local alteration includes saussuritization of plagioclase, replacement of plagioclase by a fine matrix of albite and sericite, replacement of clinopyroxene by hornblende and the development of chlorite.

The Fe–Ti oxide ores of the Panzhihua intrusion contain small amounts of the same silicate minerals that occur in the gabbroic rocks as described above, but their amounts and distribution are highly variable. The silicate minerals can be highly variable, even in samples taken close together. Titanomagnetite is dominant over ilmenite in the ores, as in the gabbros and oxide-gabbros in the same stratigraphic units, as described above. The ores with low silicate contents are characterized by a massive granular texture consisting of medium to coarse polygonal grains of titanomagnetite and ilmenite, with typical sizes ranging between 1 and 1·5 mm (Fig. 5b). Most boundaries between titanomagnetite and ilmenite are straight to slightly curved and meet at distinct triple junctions with ~120° interfacial angles. Some ores contain appreciable amount of silicates as aggregates and/or isolated grains set in a matrix of titanomagnetite and ilmenite (Fig. 5c). These have oxide grains that are smaller than those in the massive oxide ores but with the same granular polygonal texture and ~120° triple junctions. Silicate minerals

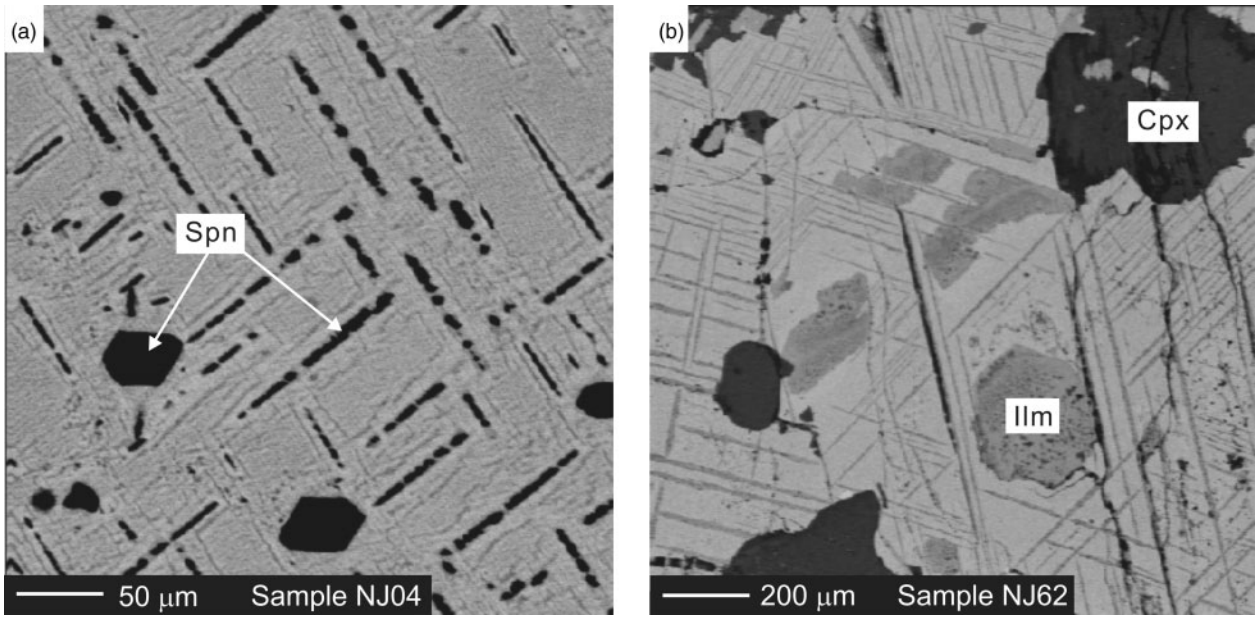

Fig. 6. Backscattered electron images of the Panzhihua oxides. (a) Blebs and lamellae of hercynitic spinel lying on the (100) planes of the magnetite host in oxide-gabbro; the presence of a fine pattern of ulvöspinel micro-intergrowths on the same plane of the host should also be noted. (b) Ilmenite lamellae lying on the (111) planes of the magnetite host in gabbro resulting in a trellis texture (Haggerty, 1976, 1991); the presence of irregular ilmenite patches thought to have resulted from granule oxy-exsolution should also be noted.

present in them commonly contain euhedral or anhedral titanomagnetite inclusions (Fig. 5d).

OXIDE MICROTEXTURES

The Panzhihua titanomagnetite contains three types of micro-intergrowths: (1) a fine pattern of ulvöspinel lamellae along the (100) planes of the host, generally similar to the cloth microtexture first noted by Ramdohr (1953); (2) blebs and lamellae of hercynitic spinel along the (100) planes in the cores of the host; (3) ilmenite lamellae along the (111) planes of the host that comprise the trellis, sandwich, and composite types noted by Haggerty (1976, 1991). The occurrence of different types of micro-intergrowths is a function of the oxide content of the rocks. The cloth microtexture is dominant in the ores and oxide-gabbros (Fig. 6a); ilmenite lamellae are present only in some grains. The trellis, sandwich, and composite textures are dominant in the gabbros (Fig. 6b). Granular ilmenite is generally free from micro-intergrowths. Fine, discrete grains of green hercynitic spinel are present in places along titanomagnetite grain boundaries.

ANALYTICAL METHODS

Samples were collected from the MGZ, LZ and MZ horizons of the Panzhihua intrusion in the Lanjiahuoshan opencast mine. The locations of samples were projected onto a SE–NW straight line on a topographic map and the respective heights were obtained after correction of the dip of the igneous layering. These values are in good agreement with those in a previous study by Zhou *et al.* (2005). Mining activity does not expose the UZ, which was instead sampled along a roadcut section.

Oxide minerals were analyzed by wavelength-dispersive spectrometry using a Cameca SX50 electron microprobe at The University of South Carolina, USA. The analyses were performed using a focused electron beam, an accelerating voltage of 15 kV and a current of 10 nA. Peak and background counting times were 30 s and 15 s, respectively. The cores of grains containing a fine pattern of exsolution textures were analyzed such that any submicroscopic intergrowths were incorporated into the analyses. Exsolved phases that are large enough for microprobe analysis were analyzed separately. Analyses of V in representative samples were corrected for the overlap of Ti Kβ and V Kα using the technique of Wright & Lovering (1965) and Carmichael (1967). The standards used include spinel for Mg and Al, diopside for Si, ilmenite for Ti, chromite for Cr, magnetite for Fe, manganese oxide for Mn and niccolite (NiAs) for Ni. Repeated analyses of optically homogeneous titanomagnetite grains and laboratory standards suggest the precision is better than ±2% relative for most elements. Ferrous and ferric iron were estimated from stoichiometry and charge balance.

RESULTS

Magnetite in rocks of the Panzhihua intrusion ranges from near end-member Fe_3O_4 to titanomagnetite containing up to 16·4 wt % TiO_2 (Table 1). The abundances of minor elements are variable: Al_2O_3 ranges from 0·26 to 4·24 wt %, MgO from below detection limit (b.d.l.) to 3·48 wt %, and

Table 1: Representative analyses of magnetite from the Panzhihua intrusion

Unit:	MGZ		LZ												MZa			
Sample:	NJ01	NJ02	NJ04	NJ11	NJ12	NJ23	NJ29	NJ35	NJ38	NJ41	NJ46	NJ47	NJ51	NJ54	NJ55	NJ59	NJ60	NJ62
Height:	2·1	4·0	50·0	77·4	80·0	131·9	168·5	215·5	242·3	247·7	262·4	276·5	305·6	321·7	322·9	328·5	328·9	331·4
Rock:	Mi-gb	Mi-gb	Ox-gb	Ore	Gb	Ore	Ore	Ore	Ox-gb	Lu-gb	Gb	Ox-gb	Gb	Lu-gb	Ore	Ore	Lu-gb	Ox-gb
n:	9	9	8	10	10	12	10	10	10	8	9	10	10	7	9	6	10	6
TiO_2	5·05	5·33	13·20	15·77	10·54	15·22	16·16	16·39	11·54	4·05	6·95	5·39	0·74	5·27	10·09	14·76	6·66	12·18
Al_2O_3	3·07	2·76	2·94	3·21	3·10	3·16	3·46	2·40	2·66	2·57	1·87	1·57	0·80	2·10	3·22	2·62	3·77	2·98
Cr_2O_3	0·17	0·28	0·03	0·04	0·07	0·05	0·05	0·05	0·05	0·05	0·04	0·05	0·05	0·10	0·05	0·09	0·11	0·05
V_2O_3	0·41	n.d.	n.d.	n.d.	0·52	0·46	0·46	n.d.	n.d.	n.d.	n.d.	n.d.	0·75	n.d.	n.d.	n.d.	n.d.	0·50
Fe_2O_3	55·64	55·28	40·21	36·15	45·29	36·47	35·44	35·19	43·59	57·71	53·28	57·27	67·00	56·18	45·99	37·99	51·02	42·16
FeO	34·41	33·70	40·66	41·90	38·71	41·83	41·10	42·86	39·80	34·83	37·45	34·20	31·71	35·20	37·13	40·45	37·00	39·53
NiO	0·09	0·09	0·02	0·02	0·02	0·04	0·03	0·03	0·02	0·04	0·03	0·03	0·06	0·04	0·02	0·02	0·02	0·03
MnO	0·26	0·29	0·45	0·55	0·40	0·60	0·46	0·43	0·45	0·16	0·21	0·27	0·06	0·28	0·36	0·44	0·33	0·38
MgO	0·93	1·43	1·68	2·50	1·37	2·02	3·33	2·10	1·15	0·09	0·18	1·21	0·17	0·46	2·06	2·61	0·20	1·74
Total	100·03	99·16	99·20	100·16	100·03	99·84	100·49	99·45	99·25	99·50	100·01	99·97	101·34	99·63	98·91	98·97	99·11	99·55
Ti	0·14	0·15	0·37	0·43	0·30	0·42	0·44	0·46	0·33	0·12	0·20	0·15	0·02	0·15	0·28	0·41	0·19	0·34
Al	0·14	0·12	0·13	0·14	0·14	0·14	0·15	0·10	0·12	0·11	0·08	0·07	0·04	0·09	0·14	0·11	0·17	0·13
Cr	0·01	0·01	0·00	0·00	0·00	0·00	0·00	0·00	0·00	0·00	0·00	0·00	0·00	0·00	0·00	0·00	0·00	0·00
V	0·01				0·01	0·01	0·01						0·02					0·01
Fe^{3+}	1·57	1·56	1·13	0·99	1·27	1·01	0·97	0·98	1·23	1·65	1·51	1·62	1·92	1·60	1·29	1·06	1·45	1·18
Fe^{2+}	1·08	1·06	1·26	1·28	1·21	1·29	1·25	1·33	1·25	1·11	1·18	1·08	1·01	1·12	1·16	1·25	1·17	1·23
Ni	0·00	0·00	0·00	0·00	0·00	0·00	0·00	0·00	0·00	0·00	0·00	0·00	0·00	0·00	0·00	0·00	0·00	0·00
Mn	0·01	0·01	0·01	0·02	0·01	0·02	0·01	0·01	0·01	0·01	0·01	0·01	0·00	0·01	0·01	0·01	0·01	0·01
Mg	0·05	0·08	0·09	0·14	0·08	0·11	0·18	0·12	0·06	0·00	0·01	0·07	0·01	0·03	0·11	0·14	0·01	0·10
Total	3·00	3·00	3·00	3·00	3·00	3·00	3·00	3·00	3·00	3·00	3·00	3·00	3·00	3·00	3·00	3·00	3·00	3·00

Unit:	MZa									MZb			UZ						
Sample:	NJ66	NJ70	NJ71	NJ77	NJ78	NJ80	NJ85	NJ91	NJ95	LR02	LR08	LR10	LR14	LR15	LR18	LR19	LR21	LR26
Height:	366·0	382·3	387·2	412·2	414·7	428·5	456·5	518·0	547·2	728·0	945·4	1056·3	1277·0	1292·0	1337·0	1352·0	1382·0	1457·0
Rock:	Gb	Ore	Ore	Ore	Gb	Ore	Gb	Lu-gb	Ox-gb	Lu-gb	Gb	Lu-gb	Gb	Ol-cpx	Gb	Ol-cpx	Lu-gb	Gb
n:	9	10	8	10	10	10	10	7	10	10	10	10	10	10	10	10	10	5
TiO_2	9·68	14·94	14·51	14·75	6·58	15·04	12·00	11·32	9·41	8·74	7·74	0·33	2·21	6·30	2·86	8·21	0·51	3·68
Al_2O_3	3·14	2·71	2·59	2·83	1·39	3·39	3·01	2·71	3·41	2·38	2·41	0·26	0·89	1·95	1·33	3·28	0·46	1·14
Cr_2O_3	0·06	0·10	0·10	0·11	0·10	0·06	0·06	0·06	0·06	0·04	0·04	0·03	0·05	0·45	0·23	2·02	0·09	0·10
V_2O_3	n.d.	n.d.	0·45	n.d.	n.d.	n.d.	n.d.	n.d.	0·64	0·37	0·44	0·50	0·64	0·56	0·62	0·54	0·66	0·71
Fe_2O_3	46·93	37·91	39·38	38·69	55·00	37·68	42·92	43·87	47·40	48·07	50·67	67·96	63·31	54·10	61·69	47·72	66·73	59·04
FeO	38·25	40·00	39·68	39·32	36·53	40·22	40·18	39·75	37·22	38·96	37·60	31·44	32·51	35·99	33·33	37·25	31·35	34·52
NiO	0·03	0·03	0·03	0·02	0·02	0·02	0·04	0·03	0·04	0·03	0·02	0·03	0·03	0·02	0·09	0·07	0·04	0·01
MnO	0·32	0·47	0·42	0·47	0·21	0·57	0·38	0·33	0·36	0·25	0·30	0·02	0·07	0·34	0·11	0·43	0·02	0·08
MgO	1·22	3·04	3·15	3·48	0·50	3·17	1·41	1·12	1·75	0·09	0·34	0·01	0·34	0·55	0·26	1·02	0·01	0·09
Total	99·63	99·21	100·31	99·69	100·33	100·16	100·00	99·19	100·29	98·93	99·56	100·59	100·05	100·27	100·54	100·53	99·86	99·37
Ti	0·27	0·41	0·40	0·41	0·19	0·41	0·33	0·32	0·26	0·25	0·22	0·01	0·06	0·18	0·08	0·23	0·01	0·11
Al	0·14	0·12	0·11	0·12	0·06	0·15	0·13	0·12	0·15	0·11	0·11	0·01	0·04	0·09	0·06	0·14	0·02	0·05
Cr	0·00	0·00	0·00	0·00	0·00	0·00	0·00	0·00	0·00	0·00	0·00	0·00	0·00	0·01	0·01	0·06	0·00	0·00

(continued)

Table 1: Continued

Unit:	MZa									MZb			UZ					
Sample:	NJ66	NJ70	NJ71	NJ77	NJ78	NJ80	NJ85	NJ91	NJ95	LR02	LR08	LR10	LR14	LR15	LR18	LR19	LR21	LR26
Height:	366·0	382·3	387·2	412·2	414·7	428·5	456·5	518·0	547·2	728·0	945·4	1056·3	1277·0	1292·0	1337·0	1352·0	1382·0	1457·0
Rock:	Gb	Ore	Ore	Ore	Gb	Ore	Gb	Lu-gb	Ox-gb	Lu-gb	Gb	Lu-gb	Gb	Ol-cpx	Gb	Ol-cpx	Lu-gb	Gb
n:	9	10	8	10	10	10	10	7	10	10	10	10	10	10	10	10	10	5
V			0·01						0·02	0·01	0·01	0·01	0·02	0·01	0·02	0·01	0·02	0·02
Fe^{3+}	1·32	1·05	1·09	1·06	1·56	1·03	1·20	1·24	1·32	1·38	1·45	1·96	1·83	1·54	1·77	1·34	1·94	1·71
Fe^{2+}	1·19	1·23	1·21	1·20	1·15	1·22	1·24	1·25	1·15	1·24	1·19	1·01	1·04	1·14	1·06	1·16	1·01	1·11
Ni	0·00	0·00	0·00	0·00	0·00	0·00	0·00	0·00	0·00	0·00	0·00	0·00	0·00	0·00	0·00	0·00	0·00	0·00
Mn	0·01	0·01	0·01	0·01	0·01	0·02	0·01	0·01	0·01	0·01	0·01	0·00	0·00	0·01	0·00	0·01	0·00	0·00
Mg	0·07	0·17	0·17	0·19	0·03	0·17	0·08	0·06	0·10	0·00	0·02	0·00	0·02	0·03	0·01	0·06	0·00	0·01
Total	3·00	3·00	3·00	3·00	3·00	3·00	3·00	3·00	3·00	3·00	3·00	3·00	3·00	3·00	3·00	3·00	3·00	3·00

MGZ, Marginal zone; LZ, Lower zone; MZa, Middle zone a; MZb, Middle zone b; UZ, Upper zone; Mi-gb, microgabbro; Gb, gabbro; Lu-gb, leucogabbro; Ox-gb, oxide gabbro; Ore, Fe–Ti oxide ore; Ol-cpx, olivine clinopyroxenite. n.d., not determined; n, number of analysis.

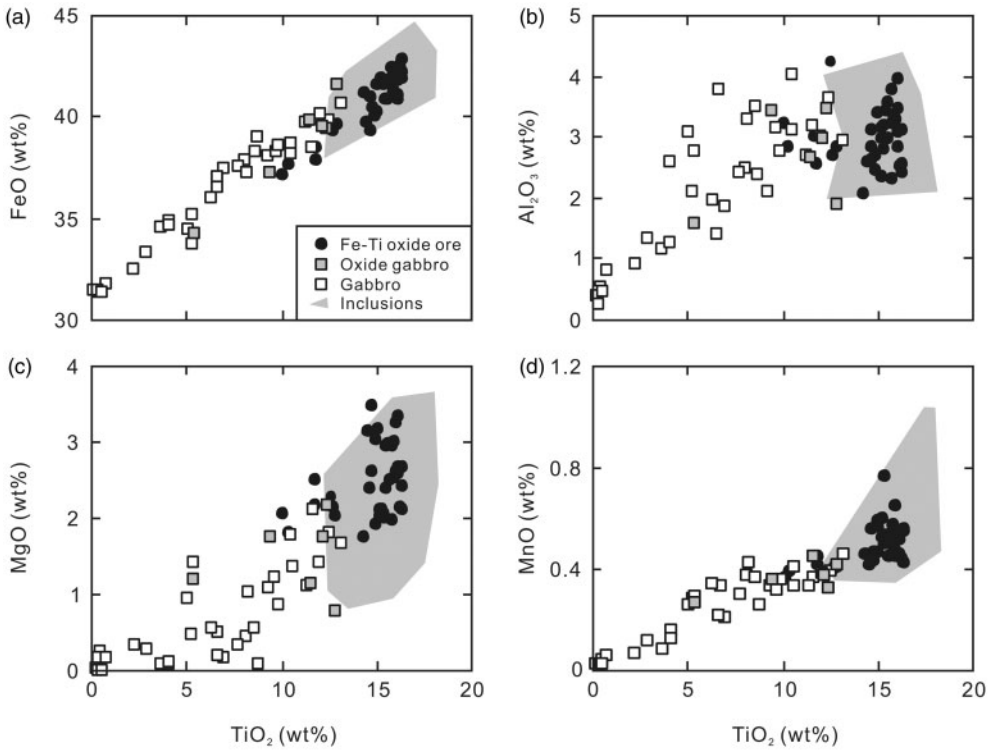

Fig. 7. Binary plots of concentrations of major elements vs TiO_2 for magnetite in the Panzhihua intrusion. (a) FeO; (b) Al_2O_3; (c) MgO; (d) MnO.

MnO from b.d.l. to 0·76 wt %. Magnetite compositions show positive correlations of Al_2O_3, MgO, MnO and FeO with TiO_2, with the highest abundances in magnetite in the Fe–Ti oxide ores (Fig. 7). Titanomagnetite inclusions in plagioclase and clinopyroxene are compositionally similar to those present in the Fe–Ti oxide ores (Table 2, Fig. 7). Granular ilmenite ranges from end-member $FeTiO_3$ to ferrian ilmenite containing 7·9 wt % Fe_2O_3 (Table 3).

Table 2: Representative analyses of titanomagnetite inclusions hosted in clinopyroxene and plagioclase

Unit:	LZ														MZ			
Sample:	NJ05	NJ05	NJ05	NJ05	NJ07	NJ07	NJ12	NJ18	NJ18	NJ18	NJ24	NJ32	NJ37	NJ37	NJ55	NJ57	NJ62	NJ79
Height:	53·7	53·7	53·7	53·7	57·3	57·3	80·0	102·9	102·9	102·9	140·7	192·5	233·2	233·2	322·9	325·3	331·4	419·8
Host:	Plag	Plag	Plag	Cpx	Cpx	Cpx	Cpx	Cpx	Cpx	Cpx	Cpx	Cpx	Cpx	Cpx	Cpx	Cpx	Cpx	Cpx
Grain:	core	$n=2$	$n=2$	core	core	$n=2$	$n=2$	$n=2$	$n=2$	$n=15$	$n=2$	$n=2$	$n=2$	$n=2$	$n=2$	$n=14$	$n=2$	core
TiO_2	17·02	13·53	16·92	17·70	13·43	12·80	17·83	15·81	15·62	16·08	16·15	16·14	15·79	15·57	12·50	14·08	14·22	15·25
Al_2O_3	2·19	3·30	3·65	2·37	3·13	2·09	2·16	3·94	3·16	4·26	3·74	2·90	3·24	2·25	3·95	4·06	2·84	2·99
Cr_2O_3	0·04	0·04	0·01	0·04	0·03	0·05	0·06	0·03	0·05	0·05	0·03	0·06	0·05	0·05	0·05	0·04	0·04	0·02
Fe_2O_3	33·08	39·35	32·65	33·31	39·37	41·45	32·59	34·55	35·38	34·16	34·32	35·10	34·98	36·06	40·30	37·38	38·08	36·49
FeO	43·87	40·80	44·59	41·16	41·97	40·87	43·41	40·49	41·79	40·61	41·04	43·04	41·98	43·28	38·42	39·90	41·55	41·15
NiO	b.d·3	0·08	0·01	b.d.	b.d.	b.d.	0·02	0·04	0·02	0·03	0·05	0·04	0·01	0·03	0·03	0·02	b.d.	b.d.
MnO	0·54	0·40	0·43	1·01	0·50	0·39	0·50	0·50	0·54	0·44	0·42	0·54	0·39	0·71	0·42	0·44	0·62	0·39
MgO	1·48	1·78	1·53	3·56	0·93	1·08	2·46	3·24	2·24	3·52	3·17	1·88	2·29	1·03	2·58	2·65	1·44	2·54
Total	98·21	99·31	99·82	99·15	99·37	98·75	99·03	98·62	98·81	99·16	98·94	99·75	98·73	98·99	98·27	98·61	98·78	98·88
Ti	0·48	0·38	0·47	0·49	0·38	0·36	0·50	0·44	0·44	0·44	0·44	0·45	0·44	0·44	0·35	0·39	0·40	0·42
Al	0·10	0·14	0·16	0·10	0·14	0·09	0·09	0·17	0·14	0·18	0·16	0·13	0·14	0·10	0·17	0·18	0·13	0·13
Cr	0·00	0·00	0·00	0·00	0·00	0·00	0·00	0·00	0·00	0·00	0·00	0·00	0·00	0·00	0·00	0·00	0·00	0·00
Fe^{3+}	0·94	1·10	0·90	0·92	1·11	1·18	0·91	0·95	0·99	0·94	0·95	0·97	0·98	1·02	1·13	1·04	1·07	1·02
Fe^{2+}	1·38	1·26	1·37	1·26	1·31	1·29	1·35	1·24	1·30	1·24	1·26	1·33	1·30	1·36	1·19	1·23	1·30	1·27
Ni	0·00	0·00	0·00	0·00	0·00	0·00	0·00	0·00	0·00	0·00	0·00	0·00	0·00	0·00	0·00	0·00	0·00	0·00
Mn	0·02	0·01	0·01	0·03	0·02	0·01	0·02	0·02	0·02	0·01	0·01	0·02	0·01	0·02	0·01	0·01	0·02	0·01
Mg	0·08	0·10	0·08	0·19	0·05	0·06	0·14	0·18	0·12	0·19	0·17	0·10	0·13	0·06	0·14	0·15	0·08	0·14
Total	3·00	3·00	3·00	3·00	3·00	3·00	3·00	3·00	3·00	3·00	3·00	3·00	3·00	3·00	3·00	3·00	3·00	3·00

Abbreviations as for Table 1, and Plag, plagioclase; Cpx, clinopyroxene; b.d., below detection limit.

Other than Fe and Ti, Mg and Mn are the only significant elements present in the ilmenites, with 0·08–8·5 wt % MgO and 0·42–1·78 wt % MnO. Granular ilmenite in the oxide ores has higher Ti and Mg but lower Mn than that in the oxide-gabbros and gabbros. Ilmenite lamellae in titanomagnetite have compositions similar to the granular ilmenite (Table 4). Hercynitic spinel included in titanomagnetite is a solid solution between spinel *sensu stricto* and hercynite. It has 63·9–66·4 wt % Al_2O_3, 11·5–15·4 wt % FeO, and 17·9–20·8 wt % MgO, with trace amounts of Fe^{3+}, Ti and Mn (Table 5).

DISCUSSION

Primary oxide composition

Subsolidus re-equilibration and exsolution commonly mask the composition of primary Fe–Ti oxides, here defined as the oxide composition at magmatic temperatures prior to any of the above processes (Buddington & Lindsley, 1964; Frost *et al.*, 1988; Frost & Lindsley, 1991). Earlier studies attempted to obtain primary oxide composition via careful integration of exsolved phases with the host titanomagnetite in complex Fe–Ti oxide grains (Bowles, 1977; Frost & Chacko, 1989). In this section, we reconstruct the primary oxide composition for the Panzhihua intrusion using a similar technique.

We choose Fe–Ti oxide ores in the Panzhihua intrusion for the reconstruction of the primary oxide composition. The reason is that oxide minerals dominate in the ores and hence are less prone to subsolidus compositional modification imposed by the coexisting mafic silicates. We integrate compositions of hercynitic spinel intergrowths and granular ilmenite to the host titanomagnetite based on the relative abundance of these minerals. The abundance of hercynitic spinel (relative to the host titanomagnetite) was estimated by counting on a grid superimposed on backscattered electron and reflected light microscope images. Estimation of the relative proportion of primary and oxy-exsolved ilmenite is challenging because of its coarse grain size and the fact that the majority of the ilmenite occurs as discrete granules intergrown with titanomagnetite, not as lamellae within it. However, there are two lines of evidence against the presence of substantial amounts of primary ilmenite: (1) whole-rock data for

Table 3: Representative analyses of ilmenite from the Panzhihua intrusion

Unit:	MGZ	LZ								MZ				MZb	UZ		
Sample:	NJ02	NJ12	NJ04	NJ05	NJ11	NJ34	NJ42	NJ43	NJ51	NJ58	NJ71	NJ77	NJ78	LR02	LR18	LR15	LR19
Height:	4·0	80·0	50	53·7	77·4	208·6	249·6	251·3	305·6	326·8	387·2	412·2	414·7	728·0	1337·0	1292·0	1352·0
Rock:	Mi-gb	Gb	Ox-gb	Ox-gb	Ore	Ore	Lu-gb	Lu-gb	Gb	Lu-gb	Ore	Ore	Gb	Lu-gb	Gb	Ol-cpx	Ol-cpx
n:	6	8	4	5	7	2	2	2	10	4	2	2	8	6	7	8	8
TiO_2	51·45	52·01	52·50	53·53	54·08	54·73	49·15	51·26	49·38	50·97	54·57	55·29	51·69	50·04	49·74	51·34	51·34
Fe_2O_3	5·53	4·42	4·07	3·29	3·96	2·61	6·43	4·30	7·94	5·17	2·99	2·58	4·45	5·75	6·61	5·86	5·74
FeO	36·83	38·69	39·43	36·99	35·19	35·10	41·87	40·68	39·81	40·37	34·07	34·03	40·84	43·25	42·59	39·84	39·11
MnO	1·24	0·68	0·69	0·66	0·56	0·59	0·95	0·81	0·91	0·70	0·52	0·53	0·72	1·56	1·38	0·83	0·90
MgO	4·56	4·12	3·97	5·87	7·20	7·56	0·76	2·57	2·03	2·65	8·11	8·50	2·73	0·08	0·40	3·07	3·43
Total	99·62	99·91	100·65	100·34	101·00	100·59	99·16	99·61	100·08	99·86	100·27	100·92	100·43	100·67	100·71	100·94	100·52
Ti	0·63	0·64	0·64	0·65	0·64	0·65	0·63	0·64	0·62	0·63	0·65	0·65	0·64	0·63	0·62	0·63	0·63
Fe^{3+}	0·07	0·05	0·05	0·04	0·05	0·03	0·08	0·05	0·10	0·06	0·04	0·03	0·06	0·07	0·08	0·07	0·07
Fe^{2+}	0·50	0·53	0·54	0·50	0·47	0·46	0·59	0·56	0·55	0·56	0·45	0·45	0·56	0·61	0·59	0·54	0·53
Mn	0·02	0·01	0·01	0·01	0·01	0·01	0·01	0·01	0·01	0·01	0·01	0·01	0·01	0·02	0·02	0·01	0·01
Mg	0·11	0·10	0·10	0·14	0·17	0·18	0·02	0·06	0·05	0·07	0·19	0·20	0·07	0·00	0·01	0·07	0·08
Total	2·00	2·00	2·00	2·00	2·00	2·00	2·00	2·00	2·00	2·00	2·00	2·00	2·00	2·00	2·00	2·00	2·00

Abbreviations are as in Table 1.

Table 4: Compositions of ilmenite lamellae in titanomagnetite

Unit:	LZ												MZa		
Sample:	NJ04	NJ04	NJ05	NJ05	JS14	JS14	JS14	JS14	NJ39	NJ39	NJ39	NJ39	JS79	JS79	JS79
Height:	50·0	50·0	53·7	53·7					242·4	242·4	242·4	242·4			
Rock:	Ox-gb	Ox-gb	Ore	Ore	Ore	Ore	Ore	Ore	An	An	An	An	Ox-gb	Ox-gb	Ox-gb
TiO_2	52·30	51·93	53·54	53·94	54·21	53·83	54·30	54·16	51·52	51·38	51·23	51·97	52·87	53·43	53·22
Al_2O_3	0·02	0·03	0·01	0·01	0·07	0·49	0·01	0·13	0·00	0·00	0·00	0·00	0·49	0·07	0·02
Fe_2O_3	4·57	4·51	2·84	2·83	5·11	4·73	5·28	4·80	2·75	3·24	2·25	2·05	5·00	5·00	5·21
FeO	39·47	39·17	36·50	37·03	31·40	30·79	31·16	31·32	45·44	45·27	44·49	45·17	35·51	35·68	35·69
MnO	0·67	0·65	0·57	0·61	0·61	0·63	0·60	0·62	0·88	0·93	1·29	1·06	0·89	0·79	0·78
MgO	3·87	3·81	6·20	6·10	8·12	8·44	8·28	8·17	0·00	0·00	0·16	0·27	5·18	5·24	5·13
Total	100·99	100·19	99·70	100·52	99·65	99·08	99·70	99·29	100·60	100·82	99·42	100·61	100·20	100·42	100·26
Ti	0·64	0·64	0·65	0·65	0·96	0·96	0·96	0·97	0·97	0·97	0·98	0·98	0·96	0·97	0·97
Al	0·00	0·00	0·00	0·00	0·00	0·01	0·00	0·00	0·00	0·00	0·00	0·00	0·01	0·00	0·00
Fe^{3+}	0·06	0·06	0·03	0·03	0·09	0·09	0·10	0·09	0·05	0·06	0·04	0·04	0·09	0·09	0·10
Fe^{2+}	0·54	0·54	0·49	0·50	0·64	0·63	0·63	0·64	0·96	0·95	0·94	0·95	0·73	0·73	0·73
Mn	0·01	0·01	0·01	0·01	0·01	0·01	0·01	0·01	0·02	0·02	0·03	0·02	0·02	0·02	0·02
Mg	0·09	0·09	0·15	0·15	0·29	0·30	0·29	0·29	0·00	0·00	0·01	0·01	0·19	0·19	0·18
Total	2·00	2·00	2·00	2·00	2·00	2·00	2·00	2·00	2·00	2·00	2·00	2·00	2·00	2·00	2·00

Abbreviations are as in Table 1. Samples with prefix JS were collected from a different traverse than the NJ samples and heights are not given here. Ox-gb, oxide gabbro; Ore, Fe–Ti oxide ore; An, anorthosite.

Table 5: Representative analyses of hercynitic spinel hosted in titanomagnetite

Unit:	LZ										MZ				
Sample:	NJ04	NJ05	NJ08	NJ09	NJ14	NJ24	NJ27	NJ31	NJ36	NJ45	NJ47	NJ55	NJ59	NJ73	NJ79
Height:	50·0	53·7	63·8	65·7	89·5	140·7	156·0	185·6	228·6	254·8	276·5	322·9	328·5	394·8	419·8
Rock:	Ox-gb	Ox-gb	Ore	Ore	Ore	Ore	Ore	Ore	Ore	Ore	Ox-gb	Ore	Ore	Ore	Ore
TiO_2	0·44	0·38	0·41	0·51	0·60	0·54	0·61	0·46	0·23	0·40	0·36	0·25	0·19	0·37	0·31
Al_2O_3	64·92	65·27	65·92	66·35	65·68	65·88	65·91	64·95	66·13	65·47	65·91	65·46	63·90	64·64	64·81
Fe_2O_3	1·61	2·26	2·26	2·64	1·53	1·51	2·07	1·96	2·05	2·22	1·38	1·80	3·95	3·31	1·60
FeO	15·35	13·89	11·45	11·72	12·80	12·43	12·22	12·62	11·59	11·96	12·87	13·29	11·94	11·48	13·61
MnO	0·20	0·05	0·01	0·09	0·06	0·02	0·14	0·10	0·08	0·09	0·11	0·17	0·07	0·04	0·13
MgO	17·87	19·02	20·72	20·82	19·82	20·26	20·35	19·61	20·35	20·15	19·57	19·13	19·79	20·73	18·63
Total	100·40	100·86	100·76	102·14	100·49	100·65	101·30	99·69	100·44	100·29	100·19	100·09	99·84	100·57	99·10
Ti	0·01	0·01	0·01	0·01	0·01	0·01	0·01	0·01	0·00	0·01	0·01	0·00	0·00	0·01	0·01
Al	1·95	1·94	1·94	1·93	1·94	1·94	1·93	1·94	1·95	1·94	1·96	1·95	1·91	1·91	1·96
Fe^{3+}	0·03	0·04	0·04	0·05	0·03	0·03	0·04	0·04	0·04	0·04	0·03	0·03	0·08	0·06	0·03
Fe^{2+}	0·33	0·29	0·24	0·24	0·27	0·26	0·25	0·27	0·24	0·25	0·27	0·28	0·25	0·24	0·29
Mn	0·00	0·00	0·00	0·00	0·00	0·00	0·00	0·00	0·00	0·00	0·00	0·00	0·00	0·00	0·00
Mg	0·68	0·71	0·77	0·77	0·74	0·75	0·76	0·74	0·76	0·76	0·73	0·72	0·75	0·77	0·71
Total	3·00	3·00	3·00	3·00	3·00	3·00	3·00	3·00	3·00	3·00	3·00	3·00	3·00	3·00	3·00

Abbreviations are as in Table 1.

rocks of the Panzhihua intrusion from Zhou *et al.* (2005) indicate that the bulk ore has ~16 wt % TiO_2, which is similar to the most ulvöspinel-rich magnetite in the ores; (2) silicate minerals contain inclusions of titanomagnetite but lack ilmenite (e.g. Table 2).

Based on the estimated titanomagnetite/hercynitic spinel ratio of ~24:1 (i.e. 4 vol. % spinel), we obtain the composition of titanomagnetite before spinel exsolution [composition (4) in Table 6]. This composition is then adjusted by the addition of ilmenite to match the average TiO_2 content of the titanomagnetite inclusions in silicate minerals that contain no sign of extensive exsolution. The resultant primary oxide is an aluminous titanomagnetite with approximately 40 wt % FeO, 34 wt % Fe_2O_3, 16·5 wt % TiO_2, 5·3 wt % Al_2O_3, 3·5 wt % MgO and 0·5 wt % MnO [composition (5) in Table 6]. This titanomagnetite has ~40 mol % ulvöspinel component.

The occurrence of aluminous titanomagnetite as the primary oxide in the Panzhihua intrusion provides a semi-quantitative constraint on the pressure at which the intrusion crystallized. The Al_2O_3 content of spinel is partly a function of pressure and partly the activity of Al in the system; high pressure generally favors the $MgAl_2O_4$ component. Recent experiments by one of the authors (D.H.L.) showed that an Fe–Ti spinel with ~5 wt % Al_2O_3 is saturated in ferrodiorites at ~5 kbar. This agrees well with the concentration of Al_2O_3 in the primary oxide listed in Table 6, implying that the Panzhihua intrusion crystallized at a pressure close to 5 kbar.

Cooling history of the Panzhihua oxides

The cooling history of the oxide minerals in the rocks of the Panzhihua intrusion can be examined on the basis of (1) inter-oxide re-equilibration, (2) oxide-silicate re-equilibration, and (3) intra-oxide re-equilibration (Frost *et al.*, 1988; Frost, 1991). Inter-oxide re-equilibration partly involves the exchange of Fe and Ti between magnetite and ilmenite, following the coupled substitution $Fe^{2+} + Ti^{4+} = 2\ Fe^{3+}$, expressed by the equilibrium

$$Fe_2TiO_4\ (\text{in magnetite}) + Fe_2O_3\ (\text{in ilmenite}) = FeTiO_3\ (\text{in ilmenite}) + Fe_3O_4\ (\text{in magnetite}).$$

This reaction proceeds to the right with decreasing temperatures, causing magnetite and ilmenite to approach their pure end-member compositions. We evaluate this reaction for the Fe–Ti oxides in the Panzhihua intrusion using the QUILF program of Andersen *et al.* (1993). The data indicate temperatures from 500 to 650°C and fO_2 from FMQ − 1 to FMQ − 3 (where FMQ is the fayalite–magnetite–quartz buffer) that clearly mark the end of subsolidus equilibration and exsolution. Because magnetite

Table 6: Reconstruction of primary oxide composition

Nature:	Host	Exsolution		Primary oxide	
	Mt	Ilm	Spn	Mt	Mt
Remarks:	(1)	(2)	(3)	(4)	(5)
TiO_2	15·51	53·68	0·40	14·91	16·46
Al_2O_3	2·97	0·00	65·41	5·47	5·25
Fe_2O_3	36·66	4·20	2·14	35·28	34·04
FeO	41·19	34·58	12·62	40·05	39·83
MnO	0·51	0·55	0·09	0·49	0·50
MgO	2·64	7·02	19·79	3·33	3·47
Total	99·48	100·03	100·45	99·52	99·54

(1) Average composition of titanomagnetite in the ores ($n = 34$). (2) Average composition of granular ilmenite in the ores ($n = 25$). (3) Average composition of hercynitic spinel hosted in titanomagnetite ($n = 15$). (4) Composition of primary oxide adjusted for hercynitic spinel exsolution (4 vol. %). (5) Composition of primary oxide adjusted for ilmenite exsolution (4 vol. %).

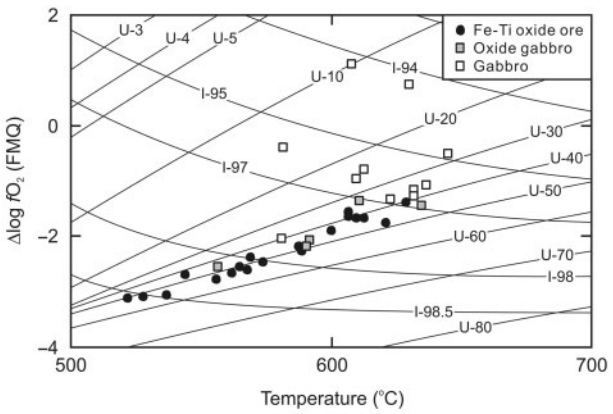

Fig. 8. $\triangle \log f O_2$–temperature diagram constructed from compositions of coexisting magnetite and ilmenite in the Panzhihua intrusion. The ilmenite and ulvöspinel isopleths are after Frost *et al.* (1988).

contains Al_2O_3 that is ignored in QUILF projections, we adjust the results manually using the expressions of Spencer & Lindsley (1981) and Lindsley & Spencer (1982). This is performed assuming that the activity of magnetite was 0·96 times the activity of magnetite in the calculations because the mole fraction of hercynite is ~0·04. The calculations indicate that the original temperatures are underestimated by <10°C and hence the effect of omission of the hercynite component is insignificant. With the exception of several samples, the data follow a near-linear array parallel to the ulvöspinel isopleths U-40 and U-50 (Fig. 8). This trend towards the convergence of the ulvöspinel isopleths is consistent with ulvöspinel exsolution in magnetite and corroborates an earlier conclusion that the primary oxide is dominated by titanomagnetite with only minor ilmenite.

Another exchange reaction that characterizes inter-oxide re-equilibration is that of Fe^{2+} and Mg between magnetite and ilmenite, expressed by the equilibrium

$$Mg^{2+}\,(\text{in magnetite}) + Fe^{2+}\,(\text{in ilmenite}) = Mg^{2+}\,(\text{in ilmenite}) + Fe^{2+}\,(\text{in magnetite}).$$

This reaction proceeds to the right with decreasing temperatures, causing ilmenite to become enriched and magnetite depleted in Mg compared with their original compositions (Pinckney & Lindsley, 1976; Lindsley, 1991). We illustrate this effect for the Panzhihua intrusion using the ores with minimal amounts of mafic silicates. Ilmenite in the ores is always richer in Mg (5·6–8·5 wt % MgO) than coexisting magnetite (1·8–3·5 wt % MgO), consistent with the generally accepted trend (Morse, 1980; Frost & Lindsley, 1991). The temperatures calculated using QUILF by allowing the Mg content of ilmenite to vary range from ~460 to 680°C, which are similar to the above blocking temperatures.

Oxide-silicate re-equilibration involves Fe–Mg exchange between Fe–Ti oxides and mafic silicates (Frost *et al.*, 1988; Frost, 1991; Frost & Lindsley, 1992). The Panzhihua intrusion has a mineral assemblage of two oxides + olivine + clinopyroxene, which allows for the use of pyroxene-QUILF in evaluating the oxide–silicate equilibrium. However, previous studies have shown that oxides tend to lose Mg to coexisting silicates on cooling (Jackson, 1969; Morse, 1980; also see Fig. 7). To minimize this effect, we estimate silica activity ($a SiO_2$) from the compositions of olivine and clinopyroxene in rocks with minimal amounts of oxides. Using QUILF, our unpublished data for olivine and clinopyroxene suggest that $a SiO_2$ clusters at ~0·6 at 1000°C and 5 kbar; this value is then used to project the oxide–silicate QUILF surface. Intersection of the U-40 isopleth and this surface marks the point at which oxide and silicate last equilibrated; this has a temperature of ~950°C and $f O_2$ between FMQ + 1 and FMQ + 1·5 (Fig. 9).

Intra-oxide re-equilibration involves the removal of Ti from titanomagnetite to ilmenite during reaction. This process commonly produces ilmenite intergrowths of different textures within magnetite and is generally referred to as oxy-exsolution (Buddington & Lindsley, 1964; Haggerty, 1976, 1991). It can be expressed by the equilibrium

$$6Fe_2TiO_4\,(\text{in magnetite}) + O_2 = 6FeTiO_3\,(\text{ilmenite}) + 2Fe_3O_4\,(\text{magnetite}).$$

This reaction proceeds to the right on cooling and requires a source of oxygen in the rock to operate (Frost, 1991). Earlier petrographic descriptions showed

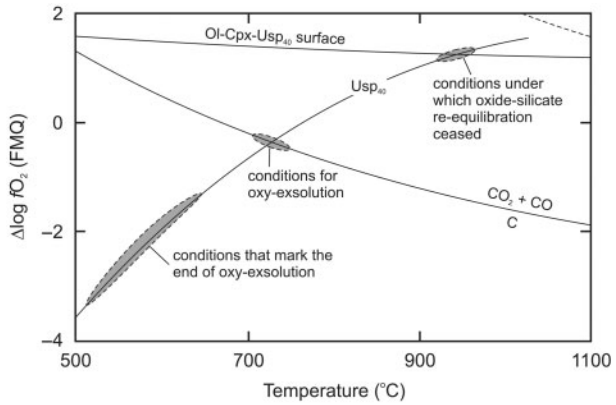

Fig. 9. $\triangle \log f\mathrm{O_2}$–temperature diagram showing inferred cooling trend for Fe–Ti oxides in the Panzhihua intrusion. The position of olivine–clinopyroxene–ulvöspinel (Ol–Cpx–$\mathrm{Usp_{40}}$) surface was estimated using the QUILF program at $a\mathrm{SiO_2} = 0{\cdot}6$. The position of the graphite saturation surface was estimated at 5 kbar after Woermann *et al.* (1977). The dotted line shows the approximate location of the R3–R3c transition in ilmenite.

that ulvöspinel intergrowths are dominant in the ores, whereas ilmenite intergrowths are dominant in the gabbros in the Panzhihua intrusion. This is consistent with the existence of a fixed proportion of 'excess' oxygen in each volume of rock. On a molecular basis, this means that there is sufficient oxygen to oxidize much of the ulvöspinel content of the magnetite in the silicate rocks, but not sufficient to do the same in the ores. Considering the strong field evidence that the Panzhihua intrusion was emplaced within limestone country rocks, the source of oxygen for oxy-exsolution is likely to be $\mathrm{CO_2}$ in carbonic fluids that dissociated from the country rocks, expressed by the reaction

$$6\mathrm{Fe_2TiO_4\,(in\ magnetite)} + \mathrm{CO_2\,(fluid)} = 6\mathrm{FeTiO_3\,(ilmenite)} + 2\mathrm{Fe_3O_4\,(magnetite)} + \mathrm{C\,(graphite)}.$$

We calculate the location of the graphite-saturation surface at 5 kbar that gives the maximum $f\mathrm{O_2}$ at which graphite may occur. Intersection of the U-40 isopleth and this surface marks the starting point of oxy-exsolution accompanied by precipitation of graphite, which has a temperature of ~700°C and $f\mathrm{O_2}$ of ~FMQ − 0·5 (Fig. 9). The molar volumes of the phases in the above reaction indicate that oxidation of 100 $\mathrm{cm^3}$ of ulvöspinel produces only 2·7 $\mathrm{cm^3}$ of graphite, presumably located on grain boundaries (see Frost *et al.*, 1989).

Figure 10 summarizes the textural modifications in rocks during cooling of the Panzhihua intrusion. In the late magmatic stage, the partially solidified oxide ores and oxide-gabbros both consist of titanomagnetite, olivine, clinopyroxene, plagioclase and intercumulus liquid (Fig. 10a and b). Oxide-silicate re-equilibration might have just ceased at this stage. On cooling, the intercumulus liquid was expelled and titanomagnetite in the ores recrystallized as coarse, polygonal grains with well-annealed junctions (Fig. 10c). The latter process was likely brought about by reduction of surface energy, supported by the fact that titanomagnetite inclusions in silicates are much smaller than magnetite grains not enclosed in any minerals. Recrystallization of titanomagnetite also occurred in the oxide-gabbro but this produced smaller grains than in the ores as a result of spatial constraints imposed by the silicate minerals (Fig. 10d). At this stage, curved oxide–silicate boundaries may have formed because there is a tendency for oxides to wet silicate boundaries (e.g. Duchesne, 1999). Exsolution of hercynitic spinel and ulvöspinel from coarsened titanomagnetite grains occurred on further cooling. In the ores, only part of the ulvöspinel component was oxidized to ilmenite, as lamellae in magnetite or discrete granules along magnetite boundaries, and the majority of the ulvöspinel remained as fine lamellae in the host magnetite (Fig. 10e). In the oxide-gabbro, much of the ulvöspinel was oxidized to ilmenite as lamellae in magnetite or discrete granules (Fig. 10f). Fine, discrete grains of hercynitic spinel also migrated to grain boundaries. Textures such as those shown in Fig. 9c–f could be used as evidence for the presence of an Fe–Ti oxide liquid (compare with Fig. 5a and c). However, we caution against interpretations based only on oxide textures, the reliability of which has been questioned (Duchesne, 1996, 1999).

Concentration of Fe–Ti oxides

A variety of mechanisms have been proposed to explain the concentration of oxides from magmas (Lister, 1966; Kolker, 1982; Duchesne, 1999). The critical question centers on whether Fe–Ti oxides are precipitated directly from magmas, or alternatively, from an Fe–Ti oxide liquid separated immiscibly from magmas. Textural evidence exists for both processes.

The mode of concentration of Fe–Ti oxides in the Panzhihua intrusion can be constrained by comparing the primary oxide compositions with the bulk oxide composition. Extrapolation of whole-rock data for the Panzhihua intrusion to 0% $\mathrm{SiO_2}$ yields 78 wt % total iron as $\mathrm{Fe_2O_3}$, 16 wt % $\mathrm{TiO_2}$, 5 wt % $\mathrm{Al_2O_3}$, and 5 wt % MgO (see Zhou *et al.*, 2005, Fig. 7). These values compare well with the estimated primary oxide composition noted in Table 6, after correction for ferrous and ferric iron. This strongly suggests that the variations in whole-rock composition can be accounted for by accumulation of Fe–Ti oxide crystals, not an oxide liquid. The reason is that in multi-component systems liquids almost always have compositions lying between those of the crystalline phases because of melting point depression. Except in the case of peritectics, liquids having the composition of a single phase lie at local temperature highs. For pure Fe–Ti oxides at least, the liquids follow cotectics, not reaction curves (e.g. Taylor, 1963), so it

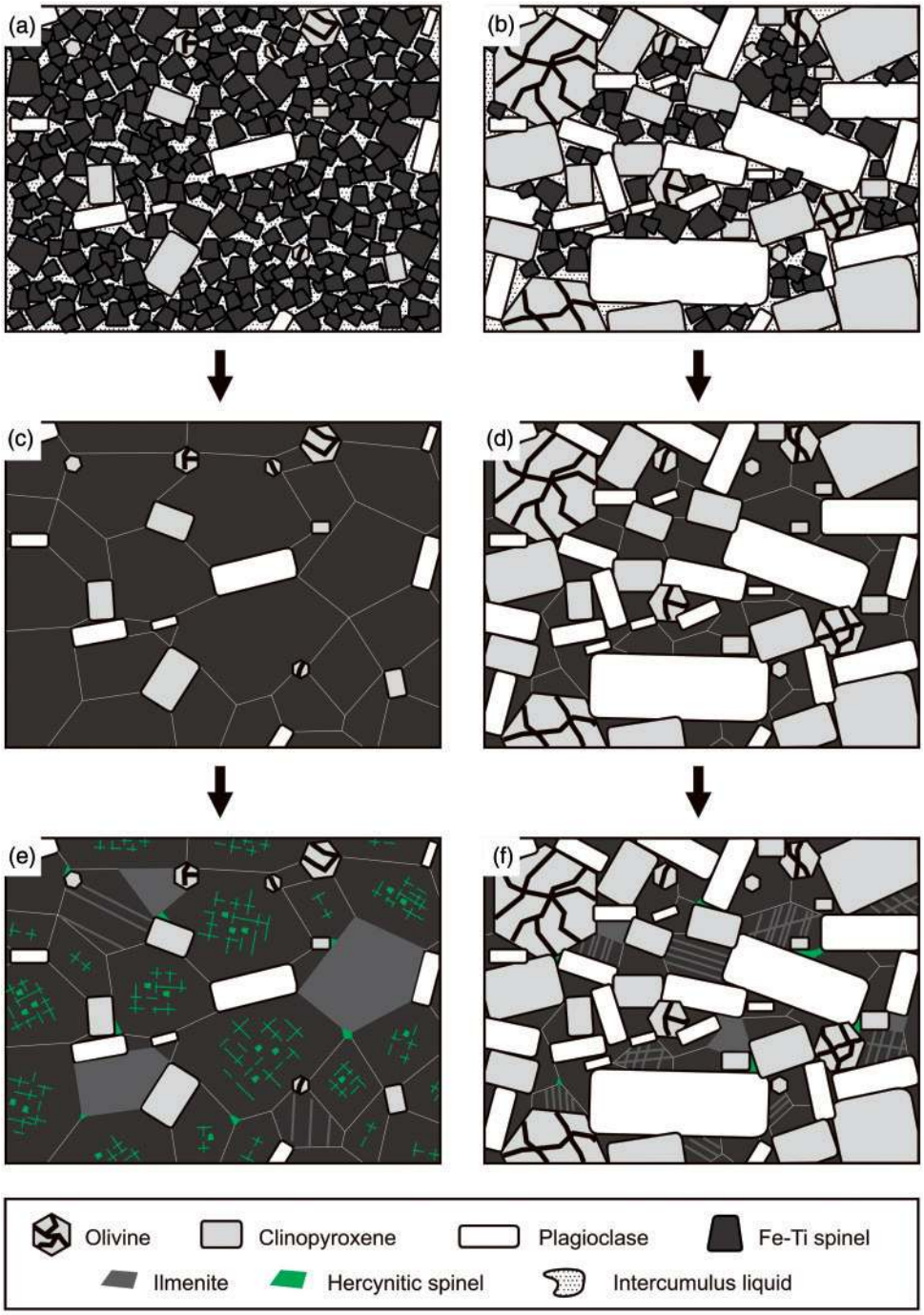

Fig. 10. Schematic diagram illustrating the crystallization sequence with progressive cooling in rocks with different oxide contents of the Panzhihua intrusion. (a, b) Partially solidified oxide ore and oxide-gabbro in the late magmatic stage. (c, d) Oxide ore and oxide-gabbro at high subsolidus temperatures. (e, f) Oxide ore and oxide-gabbro at low subsolidus temperatures. (See text for discussion.)

is much more likely that the accumulating phase was crystalline Fe–Ti oxide rather than a liquid of the same composition.

Clearly, the occurrence of oxide ores in the lower parts of the Panzhihua intrusion is best explained by gravitational settling and sorting of Fe–Ti oxide crystals, driven by the strong density contrast between Fe–Ti oxides (4·5–4·6 g/cm^3) and basaltic magma (~3·1–3·2 g/cm^3). This process demands crystallization of Fe–Ti oxides at a relatively early stage in the magma that gave rise to the

Panzhihua intrusion. Abundant and extensive oxide orebodies in the lower parts of the Panzhihua intrusion are consistent with crystal settling and sorting. Minor ore layers in the LZ and MZa may be related to magma recharge and mixing (Irvine & Sharpe, 1986), double-diffusive convection (Kruger & Smart, 1987; Tegner *et al.*, 2006), or fluctuation of fO_2 in the magma (Klemm *et al.*, 1985).

Factors controlling the formation of Fe–Ti oxide ores

The Panzhihua intrusion and its hosted Fe–Ti oxide ores allow for evaluation of the processes leading to the formation of magmatic Fe–Ti oxide ores. We draw attention to three aspects: (1) the parental magma and its differentiation; (2) fO_2; (3) the presence of volatiles. Much of the following discussion refers to the Panzhihua intrusion as an example, but the generic understanding is also relevant for Fe–Ti oxide ores associated with other mafic intrusions and Proterozoic anorthosite complexes.

The formation of Fe–Ti oxide ores in mafic intrusions can be related to a parental magma that is enriched in Fe and Ti. Such a parent might have formed: (1) as a melt that was already rich in Fe and Ti when it originated from the mantle, or (2) from a normal mantle-derived magma that became enriched in Fe and Ti as a result of differentiation prior to final emplacement, or (3) by a combination of both processes. Relatively primitive, high-Fe mantle-derived melts are best represented by ferropicrites that occur as isolated lava flows in the Precambrian or at the base of continental flood basalt provinces in the Phanerozoic (Gibson *et al.*, 2000). Tuff *et al.* (2005) demonstrated that ferropicritic magmas can be generated by melting of garnet pyroxenite under high pressure (~5 GPa) and temperature (~1550°C). This is consistent with previous experiments suggesting that the iron content of primary magmas increases with both increasing mean pressure of partial melting and increasing mean temperature at a given pressure (Langmuir & Hanson, 1980). Although rare, the occurrence of picrites with high concentrations of Fe and Ti has been documented from the ELIP (see Chung & Jahn, 1995; Zhang *et al.*, 2006). The absence of extensive olivine-rich cumulates in the Panzhihua intrusion does not suggest that the parental magma was ferropicritic, but we cannot rule out the possibility that the magma was derived from differentiation of a ferropicritic parent.

On the basis of bulk summation, Zhou *et al.* (2005) suggested that the Panzhihua intrusion crystallized from a ferrobasalt that had high Fe and Ti but low SiO_2 contents (Table 7). Although ferrobasalts are commonly rich in Fe and Ti, enrichment of these elements plus depletion in SiO_2 is rare among terrestrial basalts and most fractionated liquids derived from them (Yoder & Tilley, 1962; Kushiro, 1979). However, recent experiments by Whitaker *et al.* (2007*a*) successfully produced liquids that bracket

Table 7: Major element compositions (wt %) related to the Panzhihua intrusion

	PZH-bulk	Residual liquids of Whitaker *et al.*'s experiments			High-Ti Emeishan basalts	
Remarks:	(1)	(2)	(3)	(4)	(5)	(6)
SiO_2	42·60	45·08	43·81	41·88	44·37	45·93
TiO_2	3·99	2·47	3·37	4·57	3·15	4·86
Al_2O_3	15·80	15·90	15·35	14·62	14·95	15·65
FeO_T	15·60	13·21	14·66	15·13	13·91	13·39
MnO	0·00	0·18	0·18	0·25	0·20	0·23
MgO	5·99	6·46	5·77	5·45	7·27	7·20
CaO	11·90	9·13	8·44	8·14	10·78	7·54
Na_2O	2·45	3·04	3·25	3·02	2·26	3·27
K_2O	0·31	0·81	1·15	1·35	1·23	1·41
P_2O_5	0·69	0·50	0·75	1·27	0·34	0·51
Total	99·33	96·78	96·73	95·68	100·00	100·00
Mg-no.	45	51	45	43	52	53

(1) Composition of the Panzhihua intrusion inferred from bulk summation (Zhou *et al.*, 2005). (2), (3), (4) Representative residual liquid compositions in crystallization experiments at 9·3 kbar at 1220, 1200, and 1180°C respectively (Whitaker *et al.*, 2007*a*). (5) Representative high-Ti basalt (sample EM-78) at Ertan, ELIP (Xu *et al.*, 2001), calculated on a volatile-free basis. (6) Representative high-Ti basalt (sample RY-7) at Binchuan, ELIP (Xiao *et al.*, 2004), calculated on a volatile-free basis. FeO_T is total iron as FeO. Mg-no. = [molar $Mg/(Mg + Fe^{2+}) \times 100$], assuming 15% of total iron oxide is ferric.

Zhou *et al.*'s composition by crystallizing an olivine tholeiite at ~9·3 kbar under anhydrous conditions (~0·4 wt % H_2O) (Table 7). Whereas Fe–Ti-rich liquids can form through low-pressure differentiation of tholeiites (McBirney & Naslund, 1990; Morse, 1990; Tegner, 1997; Wiebe, 1997), enrichments in Fe and Ti combined with SiO_2 depletion appear to require high pressure. However, there is no evidence to suggest that the Panzhihua intrusion crystallized at pressure above 5 kbar. Instead, we infer that the parental magma formed by differentiation of mantle-derived melts under a pressure of ~10 kbar, probably at the base of the crust. The residual ferrogabbroic magma, enriched in Fe and Ti but poor in SiO_2, was then emplaced at a shallower depth (~5 kbar) where it crystallized to produce the Panzhihua intrusion. The above hypothesis is consistent with the occurrence of Fe–Ti-rich, SiO_2-poor ferrobasalts in the ELIP (Xu *et al.*, 2001; Xiao *et al.*, 2004) (Table 7). It is noteworthy that the proposed scenario has some similarities to the polybaric fractionation model invoked for the petrogenesis of massif anorthosites and associated jotunites and Fe–Ti–(P)

deposits (e.g. Emslie, 1985; Longhi & Ashwal, 1985). This study highlights pressure as a key factor in the generation of Fe–Ti-rich magmas and hence Fe–Ti oxide deposits.

Experiments at low pressures indicate that crystallization of Fe–Ti oxides from parental ferrobasalt is favored under relatively oxidizing conditions (Juster *et al.*, 1989; Toplis & Carroll, 1995). Periodic fluctuation of fO_2 in the magma has been postulated as the mechanism for the formation of titanomagnetite layers in the Upper Zone of the Bushveld Complex (Klemm *et al.*, 1985). Our data suggest that Fe–Ti oxides in the Panzhihua intrusion cooled along the U-40 isopleth. It is possible to extrapolate the temperature–fO_2 relations along the isopleth to magmatic conditions, provided that the oxides cooled within a closed system. At magmatic temperatures (>1000°C) along the U-40 isopleth, we obtain $fO_2 > FMQ+1{\cdot}5$ (Fig. 9). This condition is mildly oxidizing compared with most terrestrial basaltic magmas and may cause Fe–Ti oxides to be an early liquidus phase in the parental magma of the intrusion. However, we find no support for periodic fluctuation of fO_2 in the formation of oxide ores, although the possibility to form ore layers in the MZa of the intrusion exists. In addition, we draw attention to the fact that the majority of oxide ores at Panzhihua occur as thick, conformable orebodies. Fluctuation of fO_2 alone appears unlikely to produce these extensive orebodies.

One important but poorly understood aspect is the potential role of phosphorus and volatiles in the formation of Fe–Ti oxide ores. Many magmatic Fe–Ti oxide ores contain apatite as a constituent mineral, for example, nelsonites in mafic intrusions or anorthosite complexes (Kolker, 1982; von Gruenewaldt, 1993). This has caused some workers to propose that phosphorus is essential in ore formation (Philpotts, 1967). The absence of apatite in ores, combined with its presence in the silicate rocks in the upper part of the Panzhihua intrusion, suggests that phosphorus is not directly related to ore formation. However, phosphorus may play an indirect role in stabilizing Fe^{3+} in magmas and promote iron enrichment in the magma through suppression of magnetite crystallization (see Epler, 1987; Toplis *et al.*, 1994; Tollari *et al.*, 2006). We suggest that the abundance of apatite in some Fe–Ti oxide ores may be mainly fortuitous; if apatite crystallized at the same time as the oxides, it simply accumulated along with them.

Some experiments indicate that carbon and its oxides might play a role in the formation of Fe–Ti oxide ores (Weidner, 1982; Lindsley *et al.*, 1999). It is noteworthy that the wall-rocks of the Panzhihua intrusion are composed of limestone, and field evidence strongly suggests that the magma was directly emplaced into limestone. Peterson *et al.* (1999) noted that the effect of increasing solubility of Fe by dissolved carbon may be enhanced at ~5 kbar, consistent with the pressure inferred in earlier sections. However, Whitaker *et al.* (2007*b*) tested the importance of carbon by repeating their key experiments at 9·3 kbar using metal rather than graphite capsules. Their graphite-free experiments also produced Fe and Ti enrichment combined with SiO_2 depletion, demonstrating that carbon is not essential for producing such magmas. Thus, we remain speculative about the possible role of carbon in the formation of Fe–Ti oxide ores until further evidence is available.

CONCLUSION

The Panzhihua layered gabbroic intrusion (SW China) and associated Fe–Ti oxide ores provide useful constraints on the processes leading to, and the factors controlling, the formation of Fe–Ti oxide ores in mafic intrusions. This study provides definitive field and geochemical evidence that oxide ores can form by gravitational accumulation from a ferrogabbro parent magma, and by extension, from ferrodiorite. Abundant and extensive oxide orebodies in the lower parts of the Panzhihua intrusion are consistent with settling and sorting of dense titanomagnetite crystals in a magma chamber. The hypothesis that massive oxide ores formed from concentration of immiscible Fe–Ti oxide melts is not justified by the evidence obtained during this study. One important argument against liquid immiscibility is the similarity in composition between the primary oxide, reconstructed from titanomagnetite and exsolved phases in the ores, and the bulk oxide in terms of major element composition.

Effective accumulation of titanomagnetite in the Panzhihua intrusion requires its early and abundant crystallization in the parental magma of the intrusion. The proposed parental magma is rich in Fe and Ti but poor in SiO_2, features that are rare in terrestrial basalts and most fractionated liquids derived from them. Experimental evidence indicates that such liquid may represent the residual liquid that resulted from fractionation of mantle-derived magmas under anhydrous conditions and relatively high pressure (~10 kbar). Extrapolation of the U-40 isopleth, along which the Panzhihua oxides cooled, to magmatic temperatures points to mildly oxidizing conditions (~FMQ+1·5 at 1000°C). However, no evidence is found for the formation of the ores being the result of periodic fluctuation of fO_2 in the magma. The apatite-free nature of the ores in the intrusion suggests that a high concentration of phosphorus is not required for ore formation. Instead, elements such as phosphorus and carbon may promote iron enrichment in the very early stage of magma evolution until Fe–Ti oxides begin to crystallize.

ACKNOWLEDGEMENTS

The authors are grateful to Professor Yuxiao Ma for help during fieldwork. We gratefully acknowledge the helpful and constructive reviews by Tony Morse, Lewis Ashwal,

Paul Robinson and James Scoates. Their comments, along with those of editor Ron Frost, helped to improve greatly the quality of this manuscript. We also acknowledge the financial support by the Research Grant Council of Hong Kong, China (HKU7056/03P and HKU7057/05P) and The University of Hong Kong.

REFERENCES

Andersen, D. J., Lindsley, D. H. & Davidson, P. M. (1993). QUILF: A Pascal program to assess equilibria among Fe–Mg–Mn–Ti oxides, pyroxene, olivine, and quartz. *Computers and Geosciences* **19**, 1333–1350.

Ashwal, L. D. (1978). Petrogenesis of massif-type anorthosite: crystallization history and liquid line of descent of the Adirondack and Morin Complexes. PhD thesis, Princeton University, 136 pp.

Bateman, A. M. (1951). The formation of late magmatic oxide ores. *Economic Geology* **46**, 404–426.

Bowles, J. F. W. (1977). A method of tracing the temperature and oxygen-fugacity histories of complex magnetite–ilmenite grains. *Mineralogical Magazine* **41**, 103–109.

Buddington, A. F. & Lindsley, D. H. (1964). Iron–titanium oxide minerals and synthetic equivalents. *Journal of Petrology* **5**, 310–357.

Carmichael, I. S. E. (1967). The iron–titanium oxides of salic volcanic rocks and their associated ferromagnesian silicates. *Contributions to Mineralogy and Petrology* **14**, 36–64.

Charlier, B., Duchesne, J. C. & Vander Auwera, J. (2006). Magma chamber processes in the Tellnes ilmenite deposit (Rogaland Anorthosite Province, SW Norway) and the formation of Fe–Ti ores in massif-type anorthosites. *Chemical Geology* **234**, 264–290.

Chung, S.-L. & Jahn, B.-M. (1995). Plume–lithosphere interaction in generation of the Emeishan flood basalts at the Permian–Triassic boundary. *Geology* **23**, 889–892.

Duchesne, J. C. (1996). Liquid ilmenite or liquids ilmenite: a comment on the nature of ilmenite vein deposits. In: Demaiffe, D. (ed.) *Petrology and Geochemistry of Magnatic Suites of Rocks in the Continental and Oceanic Crusts*. Brussels: Université Libre de Bruxelles, pp. 73–82.

Duchesne, J. C. (1999). Fe–Ti deposits in Rogaland anorthosites (South Norway): geochemical characteristics and problems of interpretation. *Mineralium Deposita* **34**, 182–198.

Emslie, R. F. (1975). *Major rock units of the Morin complex, southwestern Quebec. Geological Survey of Canada, Paper* **74-48**, 37 pp.

Emslie, R. F. (1985). Proterozoic anorthosite massifs. In: Tobi, A. C. & Touret, J. L. R. (eds) *The Deep Proterozoic Crust in the North Atlantic Provinces*. Dordrecht: D. Reidel, pp. 39–60.

Epler, N. E. (1987). Experimental study of Fe–Ti oxide ores from the Sybille pit in the Laramie anorthosite, Wyoming. MSc thesis, State University of New York at Stony Brook, 67 pp.

Force, C. E. (1991). Geology of titanium mineral deposits. *Geological Society of America, Special Papers* **259**, 1–112.

Frost, B. R. (1991). Magnetic petrology: factors that control the occurrence of magnetite in crustal rocks. In: Lindsley, D. H. (ed.) *Oxide Minerals: Petrologic and Magnetic Significance. Mineralogical Society of America, Reviews in Mineralogy* **25**, 489–509.

Frost, B. R. & Chacko, T. (1989). The granulite uncertainty principle: limitations to thermobarometry in granulites. *Journal of Geology* **97**, 435–450.

Frost, B. R. & Lindsley, D. H. (1991). Occurrence of iron–titanium oxides in igneous rocks. In: Lindsley, D. H. (ed.) *Oxide Minerals: Petrologic and Magnetic Significance. Mineralogical Society of America, Reviews in Mineralogy* **25**, 433–468.

Frost, B. R. & Lindsley, D. H. (1992). Equilibria among Fe–Ti oxides, pyroxenes, olivine, and quartz: Part II. Application. *American Mineralogist* **77**, 1004–1020.

Frost, B. R., Lindsley, D. H. & Andersen, D. J. (1988). Fe–Ti oxide–silicate equilibria: Assemblages with fayalitic olivine. *American Mineralogist* **73**, 727–740.

Frost, B. R., Fyfe, W. S., Tazaki, K. & Chan, T. (1989). Grain-boundary graphite in rocks from the Laramie Anorthosite Complex: implications for lower crustal conductivity. *Nature* **340**, 134–136.

Gibson, S. A., Thompson, R. N. & Dickin, A. P. (2000). Ferropicrites: geochemical evidence for Fe-rich streaks in upwelling mantle plumes. *Earth and Planetary Science Letters* **174**, 355–374.

Haggerty, S. E. (1976). Opaque mineral oxides in terrestrial igneous rocks. In: Rumble, D. (ed.) *Oxide Minerals. Mineralogical Society of America, Reviews in Mineralogy* **3**, Hg101–Hg300.

Haggerty, S. E. (1991). Oxide textures. A mini atlas. In: Lindsley, D. H. (ed.) *Oxide Minerals: Petrologic and Magnetic Significance. Mineralogical Society of America, Reviews in Mineralogy* **25**, 129–219.

Irvine, T. N. & Sharpe, M. R. (1986). Magma mixing and the origin of stratiform oxide ore zones in the Bushveld and Stillwater complexes. In: Galliger, M. J., Ixer, R. A., Neary, C. R. & Prichard, H. M. (eds) *Metallogeny of Basic and Ultrabasic Rocks*. London: Institute of Mining and Metallurgy, pp. 183–198.

Jackson, E. D. (1969). Chemical variation in coexisting chromite and olivine in chromite zones of the Stillwater Complex. *Economic Geology Monograph* **4**, 41–71.

Juster, T. C., Grove, T. L. & Perfit, M. R. (1989). Experimental constraints on the generation of FeTi basalts, andesites, and rhyodacites at the Galapagos Spreading Centre, 85°W and 95°W. *Journal of Geophysical Research* **94**, 9251–9274.

Klemm, D. D., Henckel, J., Dehm, R. & von Gruenewaldt, G. (1985). The geochemistry of titanomagnetite in magnetite layers and their host rocks of the eastern Bushveld Complex. *Economic Geology* **80**, 1075–1088.

Kolker, A. (1982). Mineralogy and geochemistry of Fe–Ti oxide and apatite (nelsonite) deposits and evaluation of the liquid immiscibility hypothesis. *Economic Geology* **77**, 1146–1158.

Kruger, F. J. & Smart, R. (1987). Diffusion of trace elements during bottom crystallization of double-diffusive convection systems: The magnetitite layers of the Bushveld Complex. *Journal of Volcanology and Geothermal Research* **34**, 133–142.

Kushiro, I. (1979). Fractional crystallization of basaltic magma. In: Yoder, H. S., Jr (ed.) *The Evolution of the Igneous Rocks*. Princeton, NJ: Princeton University Press, pp. 171–203.

Langmuir, C. H. & Hanson, G. N. (1980). An evaluation of major element heterogeneity in the mantle sources of basalts. *Philosophical Transactions of the Royal Society of London, Series A* **297**, 383–407.

Lindsley, D. H. (1991). Experimental studies of oxide minerals. In: Lindsley, D. H. (ed.) *Oxide Minerals: Petrologic and Magnetic Significance. Mineralogical Society of America, Reviews in Mineralogy* **25**, 69–106.

Lindsley, D. H. & Spencer, K. J. (1982). Fe–Ti oxide geothermometry: reducing analyses of coexisting Ti-magnetite (Mt) and ilmenite (Ilm). *EOS Transactions, American Geophysical Union* **63**, Abstracts for the AGU 1982 Spring Meeting, 471.

Lindsley, D. H., Scoates, J. S., Nekvasil, H. & Dondolini, A. (1999). Dissolved carbon: A possible answer to the enigma of Fe-enriched magmas. *EOS Transactions, American Geophysical Union* **80**, S367.

Lister, G. F. (1966). The composition and origin of selected iron-titanium deposits. *Economic Geology* **61**, 275–310.

Longhi, J. & Ashwal, L. D. (1985). Two-stage model for lunar and terrestrial anorthosites: Petrogenesis without a magma ocean. In: *Proceedings of the 15th Annual Lunar and Planetary Science Conference, Part 2. Journal of Geophysical Research* **90** (Supplement), C571–C584.

Ma, Y., Liu, J. F., Wang, H. F., Mao, Y. S., Ji, X. T., Wang, D. K. & Yan, Z. Z. (2001). *Geology of the Panzhihua Region*. Chengdu: Sichuan Science and Technology Press, 367 pp. (in Chinese).

Ma, Y., Ji, X. T., Li, J. C., Huang, M. & Kan, Z. Z. (2003). *Mineral Resources of the Panzhihua Region*. Chengdu: Sichuan Science and Technology Press, 275 pp. (in Chinese).

McBirney, A. R. & Naslund, H. R. (1990). The differentiation of the Skaergaard intrusion. A discussion of Hunter and Sparks. *Contributions to Mineralogy and Petrology* **104**, 235–240.

Morse, S. A. (1980). Kiglapait mineralogy II: Fe–Ti oxide minerals and the activities of oxygen and silica. *Journal of Petrology* **21**, 685–719.

Morse, S. A. (1990). The differentiation of the Skaergaard Intrusion: A discussion of Hunter and Sparks. *Contributions to Mineralogy and Petrology* **104**, 240–244.

Peterson, A. L., Morse, S. A. & Brady, J. B. (1999). Extreme iron enrichment in graphite-saturated melts of Kiglapait Upper Zone rocks at 5 kb. *EOS Transactions, American Geophysical Union* **80**, F1096.

Philpotts, A. R. (1967). Origin of certain iron–titanium oxide and apatite rocks. *Economic Geology* **62**, 303–315.

Pinckney, L. R. & Lindsley, D. H. (1976). Effects of magnesium on iron–titanium oxides. *Geological Society of America, Abstracts with Programs* **8**, 1051.

Ramdohr, P. (1953). Ulvöspinel and its significance in titaniferous iron ores. *Economic Geology* **48**, 677–688.

Spencer, K. J. & Lindsley, D. H. (1981). A solution model for coexisting iron–titanium oxides. *American Mineralogist* **66**, 1189–1201.

Taylor, R. W. (1963). Liquidus temperatures in the system FeO–Fe_2O_3–TiO_2. *Journal of the American Ceramic Society* **46**, 276–279.

Tegner, C. (1997). Iron in plagioclase as a monitor of the differentiation of the Skaergaard intrusion. *Contributions to Mineralogy and Petrology* **128**, 45–51.

Tegner, C., Cawthorn, R. G. & Kruger, F. J. (2006). Cyclicity in the Main and Upper Zones of the Bushveld Complex, South Africa: crystallization from a zoned magma sheet. *Journal of Petrology* **47**, 2257–2279.

Tollari, N., Toplis, M. J. & Barnes, S.-J. (2006). Predicting phosphate saturation in silicate magmas: An experimental study of the effects of melt composition and temperature. *Geochimica et Cosmochimica Acta* **70**, 1518–1536.

Toplis, M. J. & Carroll, M. R. (1995). An experimental study of the influence of oxygen fugacity on Fe–Ti oxide stability, phase relations, and mineral–melt equilibria in ferro-basaltic systems. *Journal of Petrology* **36**, 1137–1170.

Toplis, M. J., Libourel, G. & Carroll, M. R. (1994). The role of phosphorus in crystallization processes of basalt: an experimental study. *Geochimica et Cosmochimica Acta* **58**, 797–810.

Tuff, J., Takahashi, E. & Gibson, S. A. (2005). Experimental constraints on the role of garnet pyroxenites in the genesis of high-Fe mantle plume derived melts. *Journal of Petrology* **46**, 2023–2058.

von Gruenewaldt, G. (1993). Ilmenite–apatite enrichments in the Upper Zone of the Bushveld Complex: A major titanium–rock phosphate resource. *International Geology Review* **35**, 987–1000.

Weidner, J. R. (1982). Iron-oxide magmas in the system Fe–C–O. *Canadian Mineralogist* **20**, 555–566.

Whitaker, M. L., Nekvasil, H., Lindsley, D. H. & Difrancesco, N. J. (2007*a*). The role of pressure in producing compositional diversity in intraplate basaltic magmas. *Journal of Petrology* **48**, 365–393.

Whitaker, M. L., Lindsley, D. H., Whitaker, J. M. K. & Nekvasil, H. (2007*b*). Carbon is not required during crystallization to produce ferrobasalts/ferrodiorites (FTP rocks). *American Mineralogist* **92**, 1750–1755.

Wiebe, R. A. (1997). Fe-rich tholeiitic liquids and their cumulate products in the Pleasant Bay layered intrusion, coastal Maine. *Contributions to Mineralogy and Petrology* **129**, 255–267.

Willemse, J. (1969). The vanadiferous magnetic iron ore of the Bushveld Igneous Complex. *Economic Geology Monographs* **4**, 187–207.

Woermann, E., Knecht, B., Rosenhauer, M. & Ulmer, G. C. (1977). The stability of graphite in the system C–O (extended abstract). In: Boyd, F.R. & Meyer, H.O.A. (eds) *The Mantle Sample: Inclusions in Kimberlites and Other Volcanics*. Santa Fe, NM: Bishop's Lodge, 423 pp.

Wright, J. B. & Lovering, J. F. (1965). Electron-probe micro-analysis of the iron–titanium oxides in some New Zealand ironsands. *Mineralogical Magazine* **35**, 604–621.

Xiao, L., Xu, Y. G., Mei, H. J., Zheng, Y. F., He, B. & Pirajno, F. (2004). Distinct mantle sources of low-Ti and high-Ti basalts from the western Emeishan large igneous province, SW China: implications for plume–lithosphere interaction. *Earth and Planetary Science Letters* **228**, 525–546.

Xu, Y. G., Chung, S. L., Jahn, B. M. & Wu, G. Y. (2001). Petrologic and geochemical constraints on the petrogenesis of Permian–Triassic Emeishan flood basalts in southwestern China. *Lithos* **58**, 145–168.

Yoder, H. S., Jr & Tilley, C. E. (1962). Origin of basalt magmas: an experimental study of natural and synthetic rock systems. *Journal of Petrology* **3**, 342–532.

Zhang, C., Mahoney, J. J., Mao, J. & Wang, F. (2006). Geochemistry of picritic and associated basalt flows of the western Emeishan flood basalt province, China. *Journal of Petrology* **47**, 1997–2019.

Zhong, H. & Zhu, W. G. (2006). Geochronology of layered mafic intrusions from the Pan–Xi area in the Emeishan Large Igneous Province, SW China. *Mineralium Deposita* **41**, 599–606.

Zhou, M.-F., Malpas, J., Song, X.-Y., Robinson, P. T., Sun, M., Kennedy, A. K., Lesher, C. M. & Keays, R. R. (2002). A temporal link between the Emeishan large igneous province (SW China) and the end-Guadalupian mass extinction. *Earth and Planetary Science Letters* **196**, 113–122.

Zhou, M.-F., Robinson, P. T., Lesher, C. M., Keays, R. R., Zhang, C.-J. & Malpas, J. (2005). Geochemistry, petrogenesis, and metallogenesis of the Panzhihua gabbroic layered intrusion and associated Fe–Ti–V oxide deposits, Sichuan Province, SW China. *Journal of Petrology* **46**, 2253–2280.